

MOCCA-SURVEY Database I. Intermediate mass black holes in Milky Way globular clusters and their connection to supermassive black holes

Manuel Arca Sedda^{1*}, Abbas Askar², Mirek Giersz³

¹*Astronomisches Rechen-Institut, Zentrum für Astronomie, University of Heidelberg, Mönchhofstrasse 12-14, 69120, Heidelberg, Germany*

²*Lund Observatory, Department of Astronomy, and Theoretical Physics, Lund University, Box 43, SE-221 00 Lund, Sweden*

³*Nicolaus Copernicus Astronomical Center, Polish Academy of Sciences, ul. Bartycka 18, 00-716 Warsaw, Poland*

Accepted XXX. Received YYY; in original form ZZZ

ABSTRACT

In this paper we explore the interplay between intermediate-mass black holes (IMBHs) and their nursing globular clusters (GCs), taking advantage of over 2000 Monte Carlo GC models. We find that the average density of IMBHs sphere of influence can be uniquely connected to the host GCs luminosity and half-light radius via a fundamental plane. We propose a statistical approach to systematically identify potential Galactic GCs harbouring either an IMBH or a massive subsystem comprised of stellar BHs. Our models show that the IMBH is often bound to a stellar companion or a stellar BH, which can lead to tidal disruption events or to low-frequency gravitational waves. We show that GCs orbiting close to the Galactic Centre have a larger probability to witness IMBH formation during their early evolution. These low-orbit GCs can deliver several IMBHs into the galaxy innermost regions, with potential impact on both electromagnetic and GW emission. We discuss potential connections between IMBHs and SMBHs inhabiting galactic nuclei, exploring the possibility that in some cases they share similar formation pathways.

Key words: (Galaxy:) globular clusters: general – galaxies: star clusters: general – black hole physics – stars: black holes – (galaxies:) quasars: supermassive black holes

1 INTRODUCTION

Intermediate mass black holes (IMBHs) constitute an elusive class of BHs with masses in the range $10^2 - 10^5 M_\odot$ that should fill the gap between stellar-mass and supermassive BHs (see Barack et al. 2018, for a recent review). Among others, a possible scenario for IMBH formation is through repeated stellar collisions in the innermost region of very dense stellar systems (Portegies Zwart & McMillan 2000, 2007; Gaburov et al. 2008; Giersz et al. 2015; Mapelli 2016). This requirement for high stellar densities makes globular clusters (GCs) promising sites for finding IMBHs. So far, a few Galactic GCs have been considered as potentially harbouring an IMBH (Silk & Arons 1975; Bash et al. 2008; Maccarone & Servillat 2008; Lützgendorf et al. 2013b; Noyola et al. 2010; Lanzoni et al. 2013; van der Marel & Anderson 2010; Strader et al. 2012; Kamann et al. 2014; Mezcua 2017; Kızıltan et al. 2017; Askar et al. 2017b), however, there

is still no conclusive evidence for their presence in these clusters.

The presence of an IMBH is often constrained via dynamical models tailored to reproduce the observed properties of a target GC. However, dynamical IMBH signatures can be efficiently mimicked by several effects, like rotation (Zocchi et al. 2015, 2017), or the presence of a BH subsystem (BHS) in the cluster centre (Baumgardt et al. 2003; Peuten et al. 2016; Arca-Sedda 2016; Arca Sedda et al. 2018; Askar et al. 2018; Zocchi et al. 2019). In principle, kinematics of stars moving inside the putative IMBH sphere of influence, like radial velocity or proper motion, encode the information needed to describe the IMBH (Gebhardt et al. 2005; Noyola et al. 2010; van der Marel & Anderson 2010; Kamann et al. 2014). However, following the motion of stars inside the IMBH’s sphere of influence is challenging owing to their small size. Another possible technique to measure IMBH properties relies upon millisecond pulsars (MSPs) timing (D’Amico et al. 2002; Colpi et al. 2002, 2003; Ferraro et al. 2003; Kızıltan et al. 2017; Perera et al. 2017; Gieles et al. 2018). Although promising, also MSPs timing features do

* E-mail: m.arcasedda@gmail.com

not provide conclusive proof for the existence of IMBHs. Two examples widely discussed in the literature are GCs 47 Tuc (Kızıltan et al. 2017; Abbate et al. 2018; Mann et al. 2018), and NGC 6624 (Perera et al. 2017; Gieles et al. 2018).

Beside dynamical constraints, another viable possibility to “see” an IMBH inhabiting a GC centre is through accretion signatures. Potentially, an IMBH can accrete either i) stars’ debris released during a tidal disruption event, ii) pristine gas entrapped into the GC.

A tidal disruption event is triggered by stars passing too close to the IMBH, which are torn apart by tidal forces. Upon disruption, a fraction of stars’ debris fall back onto the IMBH and feed it through an accretion disc, whose emission can be seen in different bands (Miller et al. 2004; Shen & Matzner 2014).

Subsequent X-ray emission is associated to the accretion disc orbiting the IMBH. Ultra-luminous X-ray sources (ULX) are thought to be the manifestation of such kind of events (Miller & Colbert 2004). First, because the kind of emission can be explained with stellar disruption operated by a moderately massive BHs, and second because they are usually observed either in the halo of early-type galaxies or close to, but clearly distinguishable from, the centre of late-type galaxies (Colbert & Ptak 2002; Miller et al. 2004). Therefore, ULX are not necessarily associated with central supermassive black holes that inhabit galaxy nuclei.

However, it must be noted that TDEs around IMBH are not the only suitable mechanisms to explain ULX features. Indeed, in most observed cases the ULX is ascribed to emission from accreting neutron stars (NSs) (Wiktorowicz et al. 2018).

Although unique observational signatures associated with an IMBH have not yet been confirmed, several potential candidates have been observed in extragalactic globular clusters (Irwin et al. 2016; Shen 2019). One example is the TDE observed in the young cluster MGG-11 in M82 (Kaaret et al. 2001; Matsumoto et al. 2001), which can be ascribed to an IMBH of mass $\sim 1000 M_{\odot}$ (Hopman et al. 2004; Baumgardt et al. 2006). More recently, Lin et al. (2018) reported the discovery of a luminous X-ray outburst likely due to a TDE operated by an IMBH lurking in the centre of a massive star cluster at 12.5 kpc from the centre of the host, a lenticular galaxy. Such event might have originated by the disruption of a main sequence (MS) star (Chen & Shen 2018).

A TDE triggered by an IMBH can involve not only MS stars, but also white dwarf (WDs) (Haas et al. 2012; MacLeod et al. 2014; Fragione et al. 2018; Anninos et al. 2018; Kawana et al. 2018). A WD-IMBH TDE can be characterised by peculiar features, like an underluminous thermonuclear explosion compared to standard SNIa, accompanied by a soft, transient X-ray signal (Rosswog et al. 2008). Also, WD disruption can lead to combined emission of X-rays and a burst of GWs (Haas et al. 2012).

If the IMBH is accreting at a high rate, multi-band radiation can be emitted by either a hot accretion disc or jets, offering the possibility to constrain the IMBH mass via X-ray, optical and radio emission (Webb et al. 2012; Farrell et al. 2014). If the accretion rate is very low, the quiescent IMBH can appear as a radio continuum source thanks to synchrotron radio jets (Maccarone & Servillat 2008; Wrobel et al. 2018). However, so far observations of Galactic globular clusters have found no strong IMBH accretion

signatures that could conclusively confirm their existence (Tremou et al. 2018).

Along with electromagnetic emission, IMBHs are, in principle, also potential gravitational wave (GW) sources. A compact stellar remnant, like a neutron star (NS) or a stellar BH, passing sufficiently close to the IMBH can occasionally be captured on a tight binary, whose evolution is mostly driven by GW emission down to coalescence. These binaries are called intermediate-mass ratio inspirals, and are promising sources that can be observed with the next generation of spaced-borne gravitational wave detectors, like LISA (Amaro-Seoane et al. 2007; Mandel et al. 2008). Ground-based observatories like LIGO and Virgo, instead, have the potential to observe mergers in the thin layer that separate stellar-mass and IMBHs, i. e. masses $O(100 M_{\odot})$ (Abbott et al. 2017).

IMBHs can be connected to galactic nuclei, at least upon the assumption that they originally form in dense clusters. Indeed, star clusters are expected to slowly segregate toward galaxy centres due to dynamical friction, possibly contributing the formation of a nuclear cluster (Tremaine et al. 1975; Capuzzo-Dolcetta 1993; Antonini et al. 2012; Antonini 2013; Perets & Mastrobuono-Battisti 2014; Arca-Sedda & Capuzzo-Dolcetta 2014b,a). Therefore, orbitally segregated globular clusters can transport their IMBHs into the galactic centre, possibly contributing to the SMBH development and growth (Ebisuzaki et al. 2001; Portegies Zwart et al. 2006). As recently investigated in a number of papers, delivered IMBHs can interact with each other and with the central SMBH, possibly leading to the formation of tight pairs that ultimately merge and release gravitational waves (Miller & Hamilton 2002; Portegies Zwart et al. 2006; Arca-Sedda & Capuzzo-Dolcetta 2017; Arca-Sedda & Gualandris 2017; Mastrobuono-Battisti et al. 2014; Fragione et al. 2017). Interestingly, a growing number of observations suggest that we already see IMBH candidates in the Milky Way centre (Oka et al. 2017; Takekawa et al. 2017; Ballone et al. 2018; Takekawa et al. 2019), whose origin might be related to infalling clusters.

Due to the intrinsic difficulties in determining IMBHs existence, the development of reliable numerical technique capable of reproducing their formation is crucial to assess the actual probability for IMBHs to form in GCs. Recently, Giersz et al. (2015) took advantage of the MOCCA Monte Carlo code (Stodolkiewicz 1986; Giersz et al. 2008, 2013; Hypki & Giersz 2013) to create a database of over 2000 reliable GCs models. The MOCCA code features stellar evolution, taken into account via the binary stellar evolution synthesis tool BSE (Hurley et al. 2002), and few body interactions via the FEWBODY integrator (Fregeau et al. 2004). The simulations sample, called MOCCA Survey Database I, covered a wide range of initial conditions in terms of GC initial mass and concentration, orbit, metallicity, binary fraction, SNe natal kicks (Askar et al. 2017a). In nearly 20% of the simulations, Giersz et al. (2015) found the formation of IMBHs with masses in the range $10^2 - 10^5 M_{\odot}$, triggered either by multiple stellar collisions in the earliest stage of GC evolution, or by slow accretion on a stellar BH seed that dominate the GC centre. In these regards, it must be noted that the current treatment for stellar collisions in MOCCA relies upon the assumption that 100% of the star is accreted

onto the BH¹. Improvements to such limitation are underway and will be presented in a forthcoming release. As discussed in our companion paper, $\sim 13\%$ of the models contain a long-lived BH subsystem (BHS) featuring up to a few hundreds of stellar mass BHs inhabiting the GC centre (Arca Sedda et al. 2018). Exploiting the database allowed us to demonstrate that it is possible to uniquely connect BH subsystems with GCs luminosity and observed core radius via a *fundamental plane* (Arca Sedda et al. 2018).

Adapting our approach for the Milky Way GC system, we identified 29 possible targets that are, at present, harbouring $10 - 5 \times 10^2$ BHs (Askar et al. 2018, 2019). As briefly discussed in our companion paper, a fundamental plane can also be defined for GCs harbouring an IMBH (Arca Sedda et al. 2018). In this paper, we make use of the MOCCA Survey Database I to deeply explore the connections between GCs and IMBHs from the theoretical and observational point of view.

On a small scale, we study the interplay between IMBHs and stars, investigating the possible development of TDEs and the formation of GW sources. On a GC scale, we investigate the possible formation of “dark clusters”, namely GCs harbouring an IMBH that undergo an almost complete disruption, and the possible delivery of IMBHs in the Galactic Centre. On a global scale, we show that a handful scaling relations can be established between IMBH sphere of influence radius, density and mass, and the luminosity and core radius of the hosting GCs. Also, we develop a statistical technique to shortlist Galactic GCs harbouring either an IMBH or a BHS, which can be used to plan tailored observational campaigns.

The paper is organized as follows: in Section 2 we present and discuss the general properties of our IMBH sample, in Section 3 we investigate the interplay between IMBHs and their hosts, and the potential connections with SMBHs in galactic nuclei, in Section 4 we define a set of scaling relations connecting IMBHs with observational properties of the host GCs, in Section 5 we show how MOCCA models can be used to constrain the presence of an IMBH in Milky Way GCs, and in Section 6 we summarize the main results of this work.

2 GENERAL PROPERTIES OF IMBHs: INFLUENCE RADIUS AND AVERAGE DENSITY

In galactic dynamics, the dynamical effect of a MBH sitting in the centre of a galaxy nucleus is quantified via the so-called influence radius, R_{IBH} . This length scale encompasses the region of space where dynamics is substantially dominated by the MBH gravity. Indeed, R_{IBH} is defined as the radius at which the kinetic energy in the MBH surroundings equals the MBH potential well, i.e. $R_{\text{IBH}} \sim GM_{\text{IBH}}/\sigma^2$ (Peebles 1972). If the MBH host phase space is well described by an isothermal sphere, this relation implies that the influence radius encompasses twice the MBH mass (Merritt et al. 2004; Merritt 2013). From a dynamical point of view,

an IMBH sitting in the centre of a massive globular cluster (GC) represents a somehow downsized version of a galactic nucleus, thus the influence radius associated to an IMBH can be defined as such that $M_{\text{GC}}(R_{\text{IBH}}) = 2M_{\text{IBH}}$. Using the IMBH mass and the concept of sphere of influence, we define another important quantity, namely the IMBH *scale density*, $\rho_{\text{IBH}} = 2M_{\text{IBH}}/R_{\text{IBH}}^3$, i.e. the average stellar density inside the influence sphere.

In this section, we show and discuss how these quantities are connected to each others. In the following, unless otherwise stated, the quantities taken into account are extracted from GCs models at 12 Gyr. All quantities referring to 12 Gyr have no pedix, while initial values are labelled with pedix 0.

Figure 1 shows the relation between IMBH mass and influence radius. It appears evident that the majority of IMBHs in MOCCA models have masses in the range $\text{Log}(M_{\text{IBH}}/M_{\odot}) \simeq 3.5 - 4.5$ and influence radii² $R_{\text{IBH}} = 1 - 3$ pc. Apart from this, we find two sub-populations of IMBHs particularly interesting. On one hand side, a handful of models show quite small IMBHs, with masses around $100 - 5000 M_{\odot}$ and compact spheres of influence, being $R_{\text{IBH}} \lesssim 0.32$ pc. On the other hand side, a sizable fraction of models show large IMBH masses, $M_{\text{IBH}} > 10^3 M_{\odot}$, and influence radii exceeding $5 - 10$ pc. As we detail in the following, these sub-populations are characterised by a peculiar evolutionary history of the parent clusters.

We find that the $M_{\text{IBH}} - R_{\text{IBH}}$ plane is inevitably connected with the host GC initial mass M_{GC} , as shown in the bottom panel of Figure 1. Indeed, limiting the sample to GCs with initial masses above $M_{\text{GC},0} \geq 5 \times 10^5 M_{\odot}$, we find that the IMBH mass and the influence radius are connected via a tight powerlaw

$$\text{Log} M_{\text{IBH}} = A \text{Log} R_{\text{IBH}} + B, \quad (1)$$

being $A = 1.11 \pm 0.05$ and $B = 3.81 \pm 0.02$. Host GCs with a lower initial mass tend to deviate from this relation, moving toward larger influence radius. Interestingly, also the subsample of GCs having masses below $2 \times 10^5 M_{\odot}$ shows a clear $M_{\text{IBH}} - R_{\text{IBH}}$ relation, with a slope $A' = 0.95 \pm 0.15$, thus compatible with the value that we find for larger GCs.

A further step needed to connect the IMBH with its surrounding is via a suitable relation between R_{IBH} and the average stellar density inside such radius, namely ρ_{IBH} . As shown in Figure 2, ρ_{IBH} is tightly related to the influence radius via a power-law

$$\text{Log} \rho_{\text{IBH}} = A \text{Log} R_{\text{IBH}} + B, \quad (2)$$

with $A = -2.42 \pm 0.05$ and $B = 3.92 \pm 0.02$. As we show in the following section, ρ_{IBH} can be used to connect the GCs observational properties to the IMBH mass.

The processes that drive IMBH formation in MOCCA can be divided into a “FAST” and a “SLOW” scenario (Giersz et al. 2015), which mostly differ in the timescale associated with the IMBH growth. In the FAST scenario the IMBH seed forms from direct collisions between stellar mass BHs and a very massive star built-up through main sequence stars

¹ As it was shown in Giersz et al. (2015), reduction of the amount of accreted mass onto an IMBH to only 25% of the intruder mass do not have a significant effect on the IMBH mass grow rate.

² for comparison, note that Sgr A*, the Milky Way SMBH, has influence radius $R_{\text{Sgr A}^*} \sim 1.5 - 3$ pc and mass $M_{\text{Sgr A}^*} = 4 \times 10^6 M_{\odot}$.

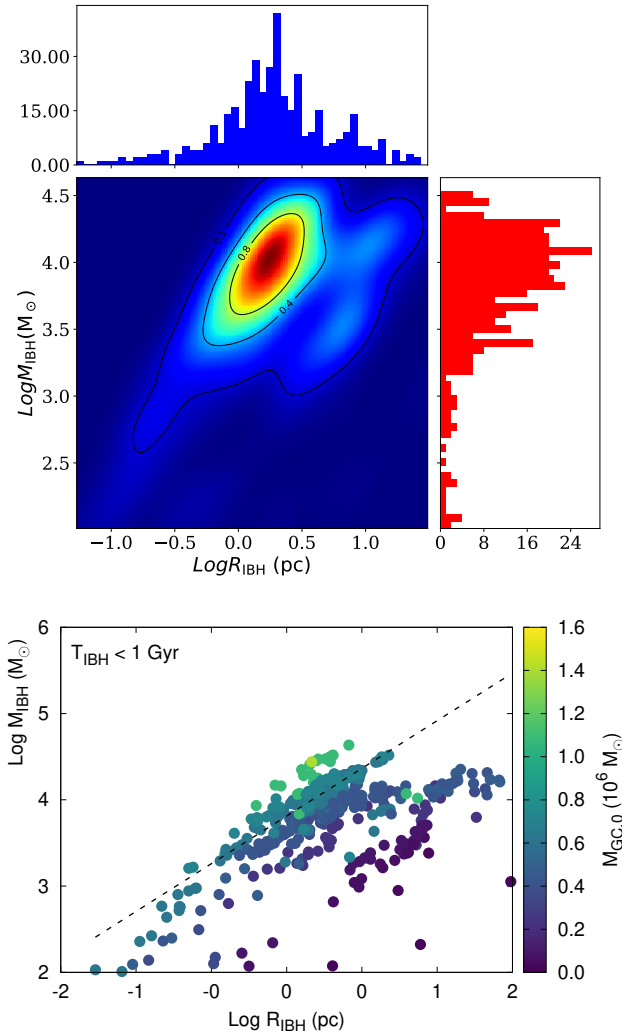


Figure 1. Top panel: IMBH mass as a function of its influence radius. Side histograms show the distribution of both quantities in our sample. Black contours identify where a fraction 0.1, 0.4, or 0.8 of all models lie. Bottom panel: same as in top panel, but we mark the host GC initial mass with different colours. The dotted line represent the best fit calculated taken into account only GCs with initial mass $M_{GC,0} \geq 5 \times 10^5 M_{\odot}$.

collisions in the early stages of the star cluster lifetime. This usually happens in star clusters with initial central densities $\sim 10^8 M_{\odot} \text{ pc}^{-3}$. As opposed to this, in the SLOW scenario the population of stellar-mass BHs is rapidly depleted via gravitational scattering until one or two BHs are left in the cluster grow. Over time-scales comparable to the GC core collapse time, the remaining BH starts growing via dynamical interactions resulting in binary mergers and mass transfer over $\gtrsim 10$ Gyr timescale.

In order to quantify how fast the IMBH seed form, we define a *formation* time scale T_{IBH} as the time at which the IMBH mass exceeds a given threshold, namely $M_{\text{IBH}} \geq 100 M_{\odot}$. Figure 3 shows how T_{IBH} varies at varying M_{IBH} and R_{IBH} . We note that IMBH mass and influence radius are taken at 12 Gyr, while T_{IBH} represents the first time

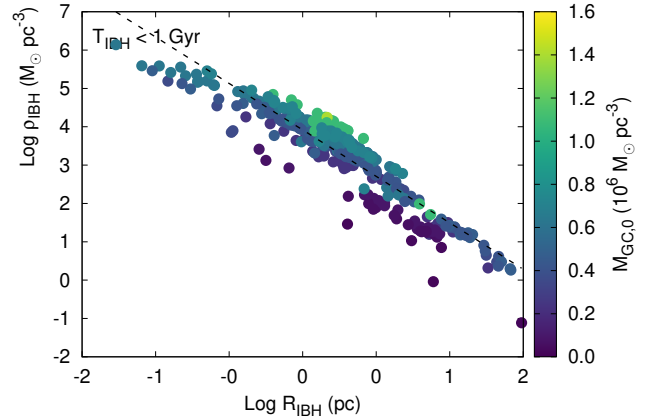


Figure 2. Stellar density ρ_{IBH} measured inside the influence radius, as a function of the influence radius. The color-coding marks the GC initial mass. Dotted black line marks the best fitting.

the IMBH mass overtake $100 M_{\odot}$. The connection between the IMBH properties and its scale time is apparent. The $M_{\text{IBH}} - T_{\text{IBH}}$ plane clearly shows a bimodal trend in the top panel of the figure, with the majority of IMBHs forming on relatively short timescales $T_{\text{IBH}} \simeq 10 - 30$ Myr. We note a weak anti-correlation, suggesting that IMBH forming via SLOW processes are lighter, on average. Also R_{IBH} shows a quite clear anti-correlation with T_{IBH} (central panel), being the sphere of influence smaller for IMBHs that form on longer timescales. Conversely, the stellar density within the influence radius increases at increasing the scale time, as seen in the bottom panel of Figure 3. This is due to the intrinsic differences between the FAST and SLOW mechanisms. Indeed, in the latter, the IMBH formation takes place after the host GC undergoes core collapse. As core collapse time scale is directly related to the GC density, IMBH forming through the SLOW scenario form in GCs that, at 12 Gyr, are characterized by relatively large densities. Conversely, in the FAST scenario the GC density is extremely high in the first stages, and trigger the rapid formation and growth of the IMBH. As the IMBH grows quickly, it shapes strongly the host GC, leading in many cases to an apparent expansion of the core, leading the GCs to have, at 12 Gyr, quite sparse matter distribution and a significant mass loss. Therefore, the three panels can be interpreted, at least in part, as a direct consequence of the dynamical effect that the IMBH has on its surroundings. An IMBH that forms on a short timescale, of the order of a few tens Myr, and reaches a mass as high as $O(1\%)$ the host GC mass represents a very efficient energy source. The net energy flux injected to passing by stars is balanced by the host GC core expansion, which triggers a decrease in the local density and reduces the interaction rate.

The presence of an IMBH in the GC centre can also affect the properties of the stellar population inhabiting its vicinity. In order to explore such effect, we calculate the average stellar mass inside the IMBH influence radius as $2M_{\text{IBH}}/N(R_{\text{IBH}})$, being $N(R_{\text{IBH}})$ the number of stars enclosed within R_{IBH} . This quantity is shown in Figure 4, as a function of the IMBH mass and the number of stars orbit-

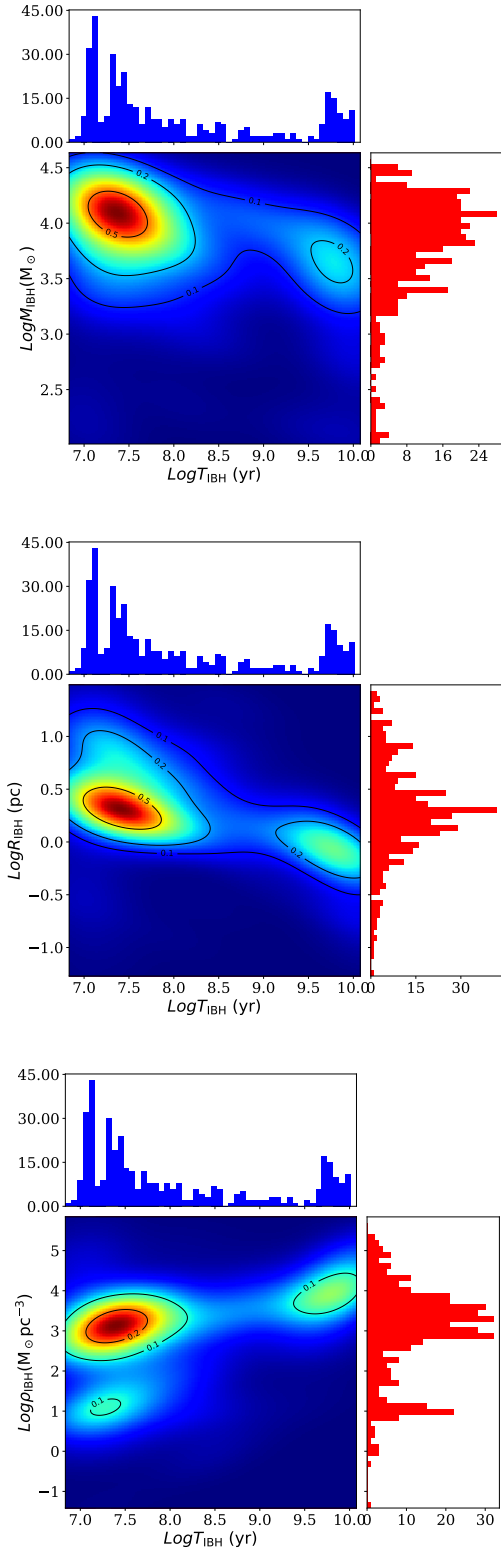


Figure 3. Time of IMBH formation as a function of the IMBH mass (top panel), influence radius (central panel) and average density (bottom panel).

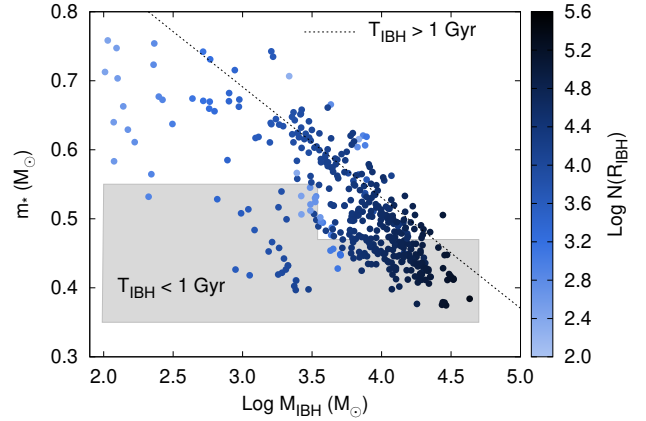


Figure 4. Average mass of stars inside the influence radius as a function of the IMBH mass. The number of stars enclosed within the IMBH influence radius is color-coded. The lower part of the shaded region contains only IMBH with $T_{\text{IBH}} < 1$ Gyr, while in the upper part both FAST and SLOW IMBH are distributed. Dotted black line identifies the scaling relation connecting m_* and the subsample of “SLOW IMBHs” ($T_{\text{IBH}} > 1$ Gyr) with mass above $M_{\text{IBH}} \geq 10^3 M_{\odot}$.

ing inside the IMBH sphere of influence. We note an evident anticorrelation between m_* and the IMBH mass. Heavier IMBHs are associated to lower m_* values, while at increasing the number of stars orbiting the IMBH the offset of such relation shifts to higher values, meaning that smaller GCs have, on average, smaller stars in the IMBH surroundings. Moreover, we find that there is a well defined region of the $M_{\text{IBH}} - m_*$ plane populated only by IMBHs with short growth time, namely ($T_{\text{IBH}} < 1$ Gyr). In the remaining part of the plane, both FAST and SLOW IMBHs coexist. If we limit our analysis to SLOW IMBHs only and assuming $M_{\text{IBH}} > 1000 M_{\odot}$, we found that the average stellar mass and the IMBHs mass are related through a powerlaw of form

$$\text{Log} \left(\frac{M_{\text{IBH}}}{M_{\odot}} \right) = -0.16 \left(\frac{m_*}{M_{\odot}} \right) + 1.18. \quad (3)$$

These results suggest that IMBHs forming quickly are, on average, associated to a lighter stellar population compared to SLOW IMBHs.

This is likely due to the fact that FAST IMBHs ($T_{\text{IBH}} < 1$ Gyr), affect dynamics over more than 10 Gyr. Interactions with the IMBH will involve the heaviest stars, which sink to the centre via mass segregation and then are kicked out via dynamical interactions. This can easily lower the average stellar mass. Conversely, SLOW IMBHs are formed after the collapse time, thus the cluster core is expected to be still dense and containing the most massive stars due to mass segregation. However, in this case IMBHs have more moderate masses, from $\sim 10^2 M_{\odot}$ to a few $10^3 M_{\odot}$.

3 IMBHs AND THEIR HOSTS

The interplay between global GCs evolution and the development of an IMBH in their centre is still partly obscure. In

this section, we try to explore the relations that link GCs evolutionary paths to the main properties of their IMBHs.

3.1 Formation of binary systems containing an IMBH

Out of the 407 MOCCA models containing an IMBH, $\sim 20\%$ of the entire MOCCA Survey database I, we serendipitously discover several models in which the IMBH is part of a binary at 12 Gyr.

Binary systems comprised of an IMBH and a close stellar companion represent one of the most promising kind of sources that can be used to directly observe the IMBH. Indeed small and repeated perturbations caused by surrounding stars can drive the companion toward an orbit that closely approaches the IMBH. Depending on its stellar type, the companion can either undergo disruption, with consequent electromagnetic emission, or be captured on an orbit that slowly spiral in due to the emission of gravitational waves until coalescence.

In the first case, the IMBH is outshined by a strong flare in the X-rays (Shen & Matzner 2014; Miller et al. 2004), followed by emission in a wide portion of the electromagnetic spectrum. Therefore, providing a comprehensive set of information about IMBHs residing in a binary has paramount importance to place constraints on a variety of astrophysical phenomena. Another important effect, not explored in this paper, arises from possible direct collisions between stars and the IMBH, which can be copious especially in the first phases of IMBH growth.

In our sample, at 12 Gyr we find 56 MS-IMBH, 66 WD-IMBH, 1 NS-IMBH and 11 BH-IMBH binaries. Figure 5 shows the mass of the components for different companion stellar types. Assuming that our models are representative of actual GC, we find that an IMBH developing in its central regions has a probability to form a binary of 32.8%, either with a MS star (13.7%), a WD (16.2%), a NS (0.2%), or a BH (2.7%). We stress here that the probability is computed taking as global sample the 407 MOCCA models that contains at 12 Gyr an IMBH with mass larger than $100 M_{\odot}$.

Interestingly, we discover IMBH paired with a MS, WD, or NS only in clusters containing no stellar BHs at 12 Gyr. This is expected by the fact that a number of stellar mass BHs orbiting around the IMBH would efficiently scatter low-mass stars, pumping energy in the IMBH surroundings and preventing its pairing with smaller stars.

This occurs in the early evolutionary phases, as BHs are the first object segregating into the cluster core due to their mass. When IMBH kicked out most of the BHs via multiple scatterings, lower mass stars migrate to the centre and start interacting with the IMBH as well. The simultaneous presence of an IMBH and a few BHs is a signature of the FAST process, as in the SLOW scenario usually all but one or two BHs are ejected before the IMBH grows up. Therefore, the absence of stellar BHs in presence of an IMBH-stellar pair has crucial observational implications. Indeed, observing a TDE associated to star disruption from an IMBH would immediately provide us with a further clue, that the host cluster with high probability does not contain stellar BHs. The orbit of GCs containing an IMBH-stellar binary are distributed in a wide range of galactocentric distances, being $R_{GC} = 1 - 30$ kpc. This suggests that TDEs triggered by an

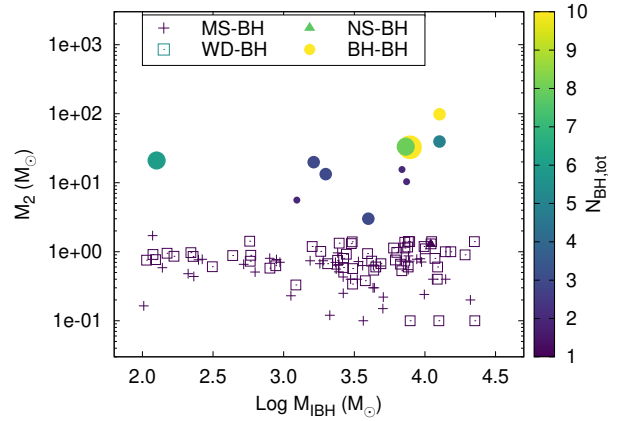


Figure 5. Upper limit to the companion mass as a function of the IMBH mass. Color-coding identifies the total number of BHs harboured in the hosting GCs at 12 Gyr. We differentiate between MS-BH (cross), WD-BH (open square), NS-BH (triangles), and BH-BH (circles) pairs. For BHs, larger circles correspond to a larger total number of BHs (single + binary), with the largest corresponding to 9 BHs and the smallest corresponding to 2.

IMBH can be seen in both the inner and outskirts of the host galaxy. Such picture is clearly compatible with both observations of ULX in the vicinity of galaxy centres and with off-centered X-ray flares, like the one recently observed by (Lin et al. 2018).

On the other hand, models containing a BH-IMBH binary are initially located at Galactocentric distances peaked around 10 kpc, except for one model for which $R_{GC} = 3$ kpc. This kind of binary are particularly interesting as they are potential GW emitters and might be observed by the next generation of GW detectors like LISA (Amaro-Seoane et al. 2007) and, at some extent, with current ground-based observatories, like LIGO (Abbott et al. 2017). In Table 1, we provide a catalogue of our BH-IMBH binaries, showing the binary masses, the total number of BHs, and the number of single and binary BHs. At 12 Gyr, we find that the number of BHs is relatively small, $N_{BH} = 2 - 9$, due to the fact that most of them are merged or kicked out during the IMBH assembly phases. The scarce BH population is characterised by a very high binary fraction, though, being the ratio between the number of binary and single BHs at 12 Gyr $N_{BHBH}/N_{BH} = (0.5 - 1)$ in all the cases. We find that BH-IMBH binaries are characterized by a broad total mass distribution in the range $M_{BH} + M_{IMBH} = (1.5 \times 10^2 - 1.3 \times 10^4) M_{\odot}$ and mass ratios $M_{BH}/M_{IMBH} = (7.6 \times 10^{-4} - 0.17)$. In all cases but one, the IMBH form via the FAST scenario over typical timescales $T_{IMBH} = 10 - 160$ Myr. In one case, the IMBH forms at a later stage, being $T_{IMBH} \simeq 10$ Gyr. This is somehow expected from the peculiar properties of the two formation channels discussed here, as in the SLOW scenario the IMBH growth starts when the BH reservoir is practically emptied, thus making more difficult for the IMBH to pair with a stellar BH.

Table 1. Main parameters of BH-IMBH binaries in MOCCA: name of the source, IMBH and BH mass, total number of BHs in the host GC at 12 Gyr, number of single and binary BHs, IMBH formation time

NAME	M_{IBH} (M_{\odot})	m_2 (M_{\odot})	N_{BH}	N_{bin}	N_{sin}	T_{IBH} (Myr)
GW01	1240.3	5.6	2	2	0	10^4
GW02	7417.5	10.4	2	2	0	12.4
GW03	6881.0	15.5	2	2	0	157.1
GW04	1630.8	19.8	3	2	1	12.8
GW05	1984.6	13.3	3	2	1	10.7
GW06	3972.4	3.0	3	2	1	10.3
GW07	12699.0	98.1	4	2	2	21.9
GW08	12684.0	39.5	4	2	2	21.6
GW09	126.0	21.0	5	4	1	9.9
GW10	7312.0	33.3	7	4	3	35.4
GW11	7835.0	32.6	9	6	3	23.2

3.2 On the IMBH dynamical influence on the host evolution: Globular versus Dark Clusters

In order to obtain a straightforward set of relations that can be used to place constraints on the presence of an IMBH in observed GCs, we need to explore the host properties at present time³. Figure 6 shows how the IMBH mass correlates with the host cluster central density at 12 Gyr. In the figure we divide the GCs sample in three population, according to different ranges of present-day mass values: $M_{\text{GC}} < 10^3 M_{\odot}$, $10^3 < M_{\text{GC}}/M_{\odot} < 10^4$, $M_{\text{GC}} > 10^4 M_{\odot}$. If we restrict the analysis to the population of clusters that preserve a mass compatible with GCs typical masses, i.e. $M_{\text{GC}} > 10^4 M_{\odot}$, we find a tight correlation that allows to convert the GC central density to the IMBH mass, being

$$\text{Log} M_{\text{IBH}} = \alpha \text{Log} \rho_{\text{GC}} + \beta, \quad (4)$$

with $\alpha = 0.295 \pm 0.009$ and $\beta = 0.96 \pm 0.09$.

Clusters that deviate from this relation are particularly interesting, as in these systems internal processes, stellar evolution, and the IMBH dynamical influence caused a very efficient mass removal. As a consequence, GCs outside the sequence are characterised by an IMBH-to-GC mass ratio very high, being $M_{\text{IBH}}/M_{\text{GC}} > 0.1 - 1$. We can define these “dark clusters”, as their stellar mass is comparable to the mass in dark remnants (see also Askar et al. 2017b). As outlined in the central panel, dark clusters are characterised by lower values of the central surface brightness, compared to normal GCs. Different behaviours are also associated to different IMBH formation channels. As shown in the bottom panel of Figure 6, GCs that undergo FAST IMBH growth and with masses at 12 Gyr below $M_{\text{GC}} < 5 \times 10^4 M_{\odot}$ significantly deviate from the relation. Such deviation seems much less significant for GCs hosting “SLOW” IMBHs, although in this case the number of small final GC masses is evidently smaller. This is due again to the fact that a SLOW IMBH form right after GC core collapse, thus implying that the IMBH is only a small fraction of the host total mass, even

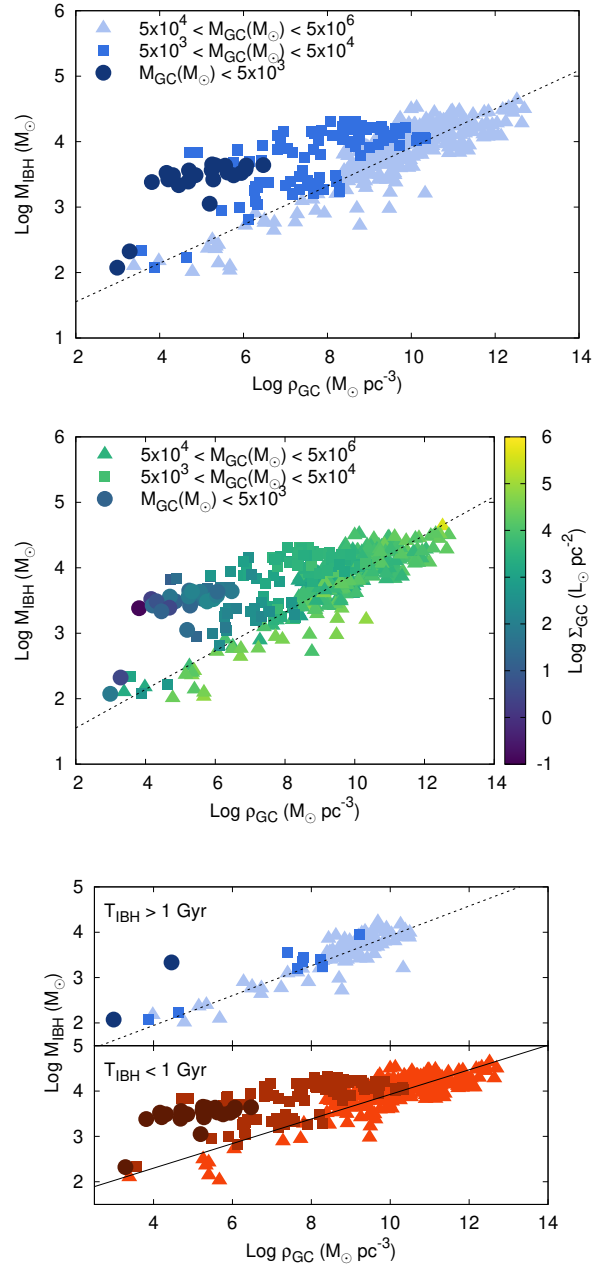


Figure 6. Top panel: IMBH mass as a function of the GC present-day central density. Different colors label different GC mass ranges: $M_{\text{GC}} < 10^3 M_{\odot}$ (dark blue), $10^3 < M_{\text{GC}}/M_{\odot} < 10^4$ (blue), $M_{\text{GC}} > 10^4 M_{\odot}$ (light blue). Central panel: same as above, but in this case we use color-coding to identify GCs surface brightness calculated at 12 Gyr. Bottom panel: same as above, but dividing the population into SLOW $T_{\text{IBH}} > 1 \text{ Gyr}$ and FAST IMBHs $T_{\text{IBH}} < 1 \text{ Gyr}$. In all panels, the dotted black line marks the best fit of the subsample of models having $M_{\text{GC}} > 10^4 M_{\odot}$.

³ We assume $t = 12 \text{ Gyr}$ as present time, for coherence’s sake in comparison with previous works that used the same set of simulations.

if the cluster core collapse time is comparable to the cluster dissolution time.

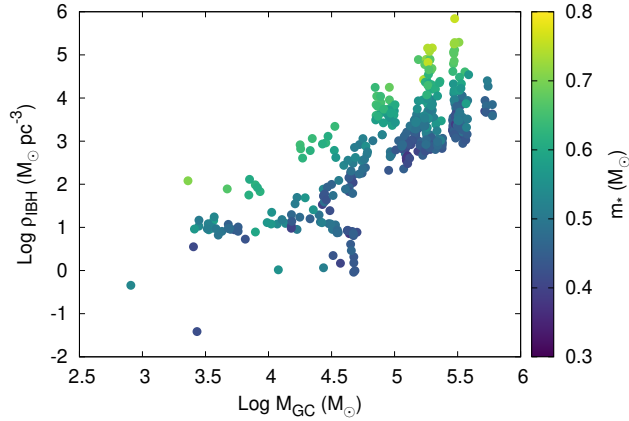


Figure 7. Stellar density inside R_{IBH} as a function of the GC mass calculated at 12 Gyr. Coloured maps identify different values of the average stellar mass.

3.3 On the delivery of IMBHs harboured in low-orbit GCs

The stellar density in the IMBH surroundings, measured through the ρ_{IBH} parameter, seems to correlate with the host cluster mass calculated at 12 Gyr, as shown in Figure 7. Although loosely tight, this relation shows that heavier GCs are expected to harbour IMBHs with denser spheres of influence. Also, at fixed the GC mass, the larger the ρ_{IBH} the heavier the average stellar mass measured within R_{IBH} and the smaller the sphere of influence.

Figure 8 shows one of the basic properties, namely the IMBH-to-GC mass ratio measured at 12 Gyr as a function of the IMBH mass and the ratio between the final and initial value of the GC mass. In the case in which mass loss processes have a marginal impact on the GC evolution, $M_{\text{GC}} \gtrsim 0.3M_{\text{GC},0}$, the IMBH-GC mass ratio lies in the range $M_{\text{IBH}}/M_{\text{GC}} \simeq 10^{-4} - 10^{-1.5}$. However, GCs experiencing a more effective mass loss, $M_{\text{GC}} \lesssim 0.1M_{\text{GC},0}$, have two main properties: i) they produce heavy IMBHs, with masses $> (0.5-3) \times 10^4 M_{\odot}$, and ii) the IMBH mass is 90–100% the host GC mass. These are the dark clusters discussed in the previous section, i.e. a type of clusters containing more or less 10^4 stars, whose mass budget is completely dominated by the IMBH.

In Figure 9, we show the correlation between the GC Galactocentric distance and the GC final mass, normalized to its initial value. First, we note that most GCs suffering an efficient mass removal, i.e. $M_{\text{GC}} \leq 0.1M_{\text{GC},0}$, move on orbits within 1–10 kpc from the Galaxy Centre, as seen in the top panel. Second, disrupted GCs bring with them quite heavy IMBHs, with masses $M_{\text{IBH}} \simeq 10^3 - 10^4 M_{\odot}$.

The two points above can have interesting consequences for the evolution of galaxy nuclei. Indeed, as discussed in (Arca Sedda et al. 2018, see their Figure 1), several MOCCA models containing an IMBH have dynamical friction times smaller than a Hubble time, suggesting that these IMBHs can be delivered into the Galactic Centre. Following Arca-Sedda et al. (2015) (but see also Arca-Sedda & Capuzzo-Dolcetta 2014b), we calculate the dynamical friction (df) timescale for all the MOCCA models having an IMBH. We

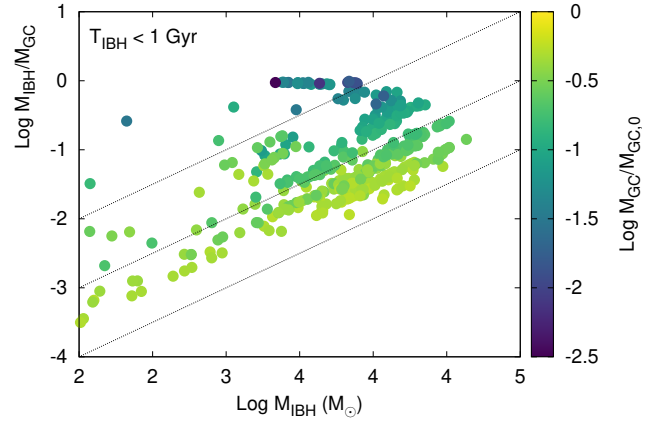


Figure 8. Ratio between the IMBH and the GC masses as a function of the IMBH mass. The colour-coding labels the final to initial GC mass ratio. Dotted lines mark the linear relation $M_{\text{IBH}}/M_{\text{GC}} \propto M_{\text{IBH}}$. All the quantities are calculated at 12 Gyr.

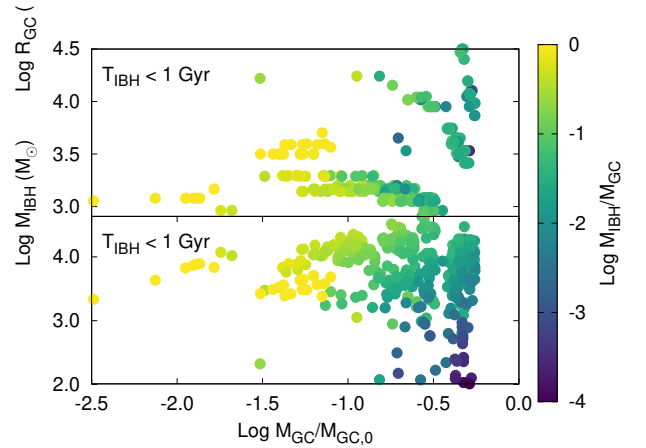


Figure 9. Galactocentric distance (top panel) and IMBH mass (bottom panel) as a function of GC mass measured at 12 Gyr, normalized to its initial value. Different colours mark the IMBH-to-GC mass ratio measured at 12 Gyr.

find 189 systems with a df time smaller than 12 Gyr. Among them, in 157 cases the IMBH growth time is much shorter than the df time, thus implying that the IMBH already grew-up when the parent cluster arrives in the Galactic Centre. Therefore, our analysis suggests that some GCs orbiting in the inner kpc of the host galaxy can witness the birth and growth of an IMBH and subsequently deliver it into the central galactic regions via df-driven inspiral. Some of these IMBHs can be wandering at present days in the MW centre, as some observations suggest (Oka et al. 2017; Takekawa et al. 2017, 2019), or might have merged in the past few Gyr with the Galactic SMBH (Arca-Sedda & Gualandris 2017). On the other hand, too many IMBHs freely orbiting the inner 10 pc would leave dynamical imprints on the nuclear cluster that are not compatible with observations (Mastrobuono-Battisti et al. 2014), thus implying that the potential number of IMBHs moving in there is most likely < 10 .

3.4 What is the connection between intermediate-mass and supermassive black holes?

As shown in the previous section, our MOCCA models show that stellar collisions, either occurring in the GC early life, or on secular time-scales, can buildup an IMBH with masses as high as a few $10^4 M_\odot$. This process allows the formation of IMBHs that perfectly fit the gap between stellar mass and supermassive black holes (SMBHs).

As for IMBHs, also the formation of supermassive black holes is a partly unsolved mystery of modern astronomy. At moment, the most credited scenario for SMBH growth are either via stellar collisions between pop III stars, or via monolithic collapse of a gaseous cloud (see Barack et al. 2018, for a review). The first scenario – mergers among pop III stars – is quite similar to what occurs in GCs harbouring an IMBH. Therefore, it might be interesting to explore whether it is possible to establish a connection between IMBHs and SMBHs. In order to compare MOCCA models with observations, we build a compilation of data available in literature for different hosts. In particular we consider:

- the sample of 13 IMBH candidates found in Galactic GCs provided by (Lützgendorf et al. 2013a);
- the sample of SMBHs and NCs that are known to co-exist in several galaxies, like the MW (Graham & Spitler 2009; Neumayer & Walcher 2012; Kormendy & Ho 2013);
- the IMBH and host cluster mass estimates provided by Lin et al. (2018), which are based on a X-ray flare originate during the tidal disruption of a passing by star;
- the compilation of bona fide IMBHs observed in a population of low-luminosity AGN (Reines & Comastri 2016; Chilingarian et al. 2018);
- a few data available for ultra-compact dwarfs (UCDs) and for the M32 compact elliptical galaxy (cE).

The aforementioned sample is shown in Figure 10. such a sample contains very different objects, likely characterized by different formation and evolution histories.

Comparing MOCCA data with the few observational constraints available for MW globulars show a relatively good agreement between models and observations, although it must be noted that the present-day GC mass in MOCCA SURVEY DATABASE I never exceeds $10^6 M_\odot$, making difficult the comparison with heavier observed GCs. Also, the population of MOCCA models containing an BHS, as defined in Arca Sedda et al. (2018), seem to complement IMBH-dominated systems, arranging in a similar region of the $M_{\text{BH}} - M_{\text{host}}$ plane.

We find two possible relations that fits relatively well MOCCA IMBHs, one leading to a connection with SMBHs in NCs

$$\text{Log} M_{\text{IBH}} = M_{11} \left(\frac{M_{\text{cl}}}{M_{\text{c1}}} + 1 \right)^\gamma \quad (5)$$

with $M_{\text{c0}} = 2 \times 10^6 M_\odot$ and $M_{10} = 5 \times 10^4 M_\odot$ (dash-dotted line in Figure 10), and the other with SMBH in low-mass AGNs:

$$\text{Log} M_{\text{IBH}} = M_{10} \text{Log} \left(\frac{M_{\text{cl}}}{M_{\text{c0}}} + 1 \right), \quad (6)$$

with $M_{11} = 1 M_\odot$, $M_{\text{c1}} = 10^4 M_\odot$, and $\gamma = 2.2$ (dotted line in Figure 10). Note that in both equations we used M_{cl} to

indicate indifferently GCs and NCs. Both relations provide a good match to observed putative IMBHs.

Regarding the IMBH-SMBH-NC connection – Equation 5 – we note that the relation provides quite a good fit also to SMBH masses in the $10^4 - 10^7 M_\odot$ region. Also, host cluster mass loss may play a role, as this mechanism is expected to be more effective in GCs than in galactic nuclei. Heavier SMBHs tend to deviate from the correlation. This might be sign of different concurrent formation processes. For low-mass SMBH, star collisions or stellar feeding onto a massive seed could have dominated the SMBH growth process, while heavier SMBH might have growth mostly because of gaseous accretion.

The IMBH-AGN connection – Equation 6 – instead, provides a good matching with galaxies hosting low-mass AGNs. We note that this relation matches the recently observed TDE event detected by Lin et al. (2018) in an extragalactic star cluster. Therefore, the relation suggests that a possible formation channel for low-mass AGN in dwarf galaxies is dominated by stellar collisions and accretion onto a heavy seed. It must be noted that such formation scenario seems to be supported also from the observational point of view, being the host of low-mass AGN all characterized by compact and bright nuclei (Chilingarian et al. 2018).

Unfortunately, MOCCA GCs in the current database have present-day masses below $\sim 10^6 M_\odot$, thus limiting the phase space region available for our analysis. Future investigations will allow us to reach larger GC masses, possibly helping in shedding light on the bridge between IMBH-SMBH. Heavier MOCCA models are currently running and under analysis. In one of them, tailored to model a NSC sitting in the centre of its host galaxy, represented with a mass $M_{\text{NSC}} = 1.31 \times 10^7 M_\odot$ and half-mass radius $r_h = 1$ pc, we find the formation of a MBH with mass $M_{\text{IBH}} = 1.21 \times 10^5 M_\odot$ (Diogo Belloni, private communication). Such point places excellently in between the scaling relation provided by Arca-Sedda (2016), connecting both BHS and IMBHs with their host masses, and the scaling relation connecting IMBHs and low-mass AGN depicted here.

4 OBSERVATIONAL SCALING RELATIONS CONNECTING IMBHs AND THEIR HOSTS

Unveiling a unique way to connect an IMBH with some observational properties of the hosting cluster represents one of the most challenging quests in modern astrophysics.

For all MOCCA models containing an IMBH, we calculated the mass to light ratio, defined as the ratio between GCs present day mass and total visual luminosity, namely M_{GC}/L_V . We find that in 25 models, i.e. $\simeq 6\%$ the sample, this quantity exceeds 10. These extremely low luminosity systems are the dark clusters discussed in the previous section.

As introduced by Arca Sedda et al. (2018), it is possible for IMBHs to define a fundamental plane, similarly to stellar BH subsystems, delimited on a side by the IMBH average density and, on the other side, by the host cluster average surface luminosity, defined as the ratio between the total visual luminosity (L_V) and the squared observational half-

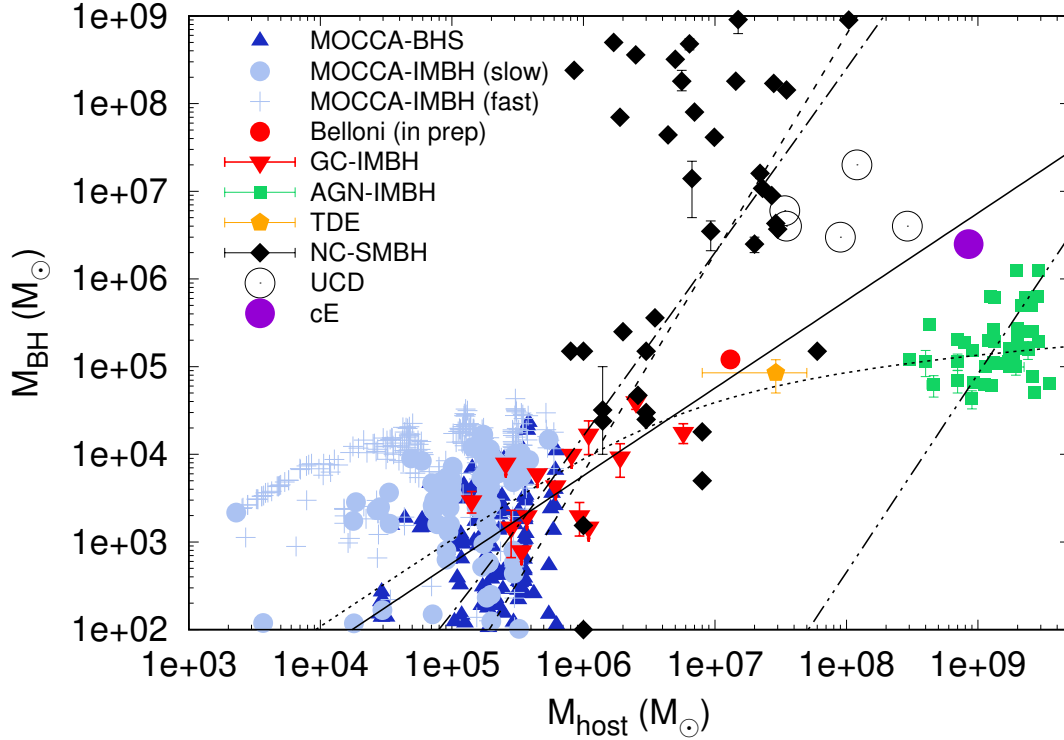


Figure 10. Central dark object mass as a function of the host mass for MOCCA models containing an IMBH (light blue filled points), or a BH subsystem (open blue points). We also add a new simulation performed with MOCCA and tailored to represent a NSC (red filled circle, Diogo Belloni, private communication). For comparison, we show the sample of Galactic GCs possibly harbouring an IMBH compiled by Lützgendorf et al. (2013a) (red triangles), a sample of galactic nuclei containing a supermassive BH (Graham & Spitler 2009; Neumayer 2012; Reines & Comastri 2016; Kormendy & Ho 2013) (black diamond), a sample of low-luminosity AGN containing bona fide IMBHs (Chilingarian et al. 2018) (green squares), and the star cluster hosting an IMBH candidate that originated the X-ray flare observed by Lin et al. (2018). We overlay the GC-BHS relation proposed by Arca-Sedda (2016) (straight black line), the BH-NC relation proposed by Graham (2016) (dashed line), the BH-bulge mass relation for low-mass galaxies (Graham 2015) (double dotted-dashed line) and two possible fits that link either GC to galactic nuclei (dash-dotted line) or to low-luminosity AGNs (dotted line).

mass radius (r_h)⁴. Figure 11 shows the fundamental plane for all the IMBHs found in MOCCA. Intriguingly, we find that the link between the GC observational properties and the IMBH density depends critically on M_{IMBH} . As shown in left panel of Figure 11, gathering the MOCCA GCs population in three distinct samples that differ in the IMBH mass range. Each sample shows a tight relation, which is steeper for the heaviest IMBHs, $M_{\text{IMBH}} > 10^4$. The fundamental relation is well fitted by a power-law, with form

$$\text{Log} \rho_{\text{IMBH}} = \alpha \text{Log} L_V / r_h^2 + \beta, \quad (7)$$

being the best-fit parameters $\alpha = 2.7 \pm 0.2$ and $\beta = -8.1 \pm 0.6$ for the heaviest IMBHs and $\alpha = 1.33 \pm 0.04$ and $\beta = -1.82 \pm 0.15$ for IMBHs in the mass range $10^3 - 10^4 M_\odot$. At a fixed L_V value, heavier IMBHs are embedded in looser spheres of influence. Fixing ρ_{IMBH} , instead, makes apparent that heavier IMBHs are hosted in more luminous clusters. The right panel in Figure 11 allows us to clarify why different IMBH mass ranges lead to a different arrangement in the fundamental plane. Indeed, the steep relation valid

for the heaviest IMBHs is populated by clusters that lost more than 70% of their initial mass. The fundamental relation for these “disrupting” clusters is much steeper compared to “surviving” clusters. This is mostly due to the fact that surviving clusters have core radii ranging in a relatively large range of values 1 – 10 pc, while their L_V values are all peaked around $10^5 L_\odot$, leading the average surface luminosity L_V / r_h^2 to increase proportionally to the square of the observational half-mass radius. Conversely, disrupting clusters have observational half-mass radii in a narrow range 1 – 2 pc and luminosities spanning a large range, thus the increase of surface average luminosity is regulated by the linear dependence on L_V . This can explain the different trends observed in the fundamental plane.

Also the IMBH formation channels play a role in shaping the fundamental plane. Indeed, SLOW IMBHs tend to follow the correlation valid for surviving clusters, while FAST IMBHs lie on both the correlations. This simply reflects the fact that, in general, SLOW IMBHs live in GCs that preserve quite a large fraction of their initial mass, while a noticeable number of FAST IMBHs develop in GCs that undergo a severe mass loss over a Hubble time.

While the fundamental plane provides a useful tool to directly connect GCs observables with the IMBH, it does not

⁴ Throughout the text we use observational half-mass radius and half-light radius indifferently

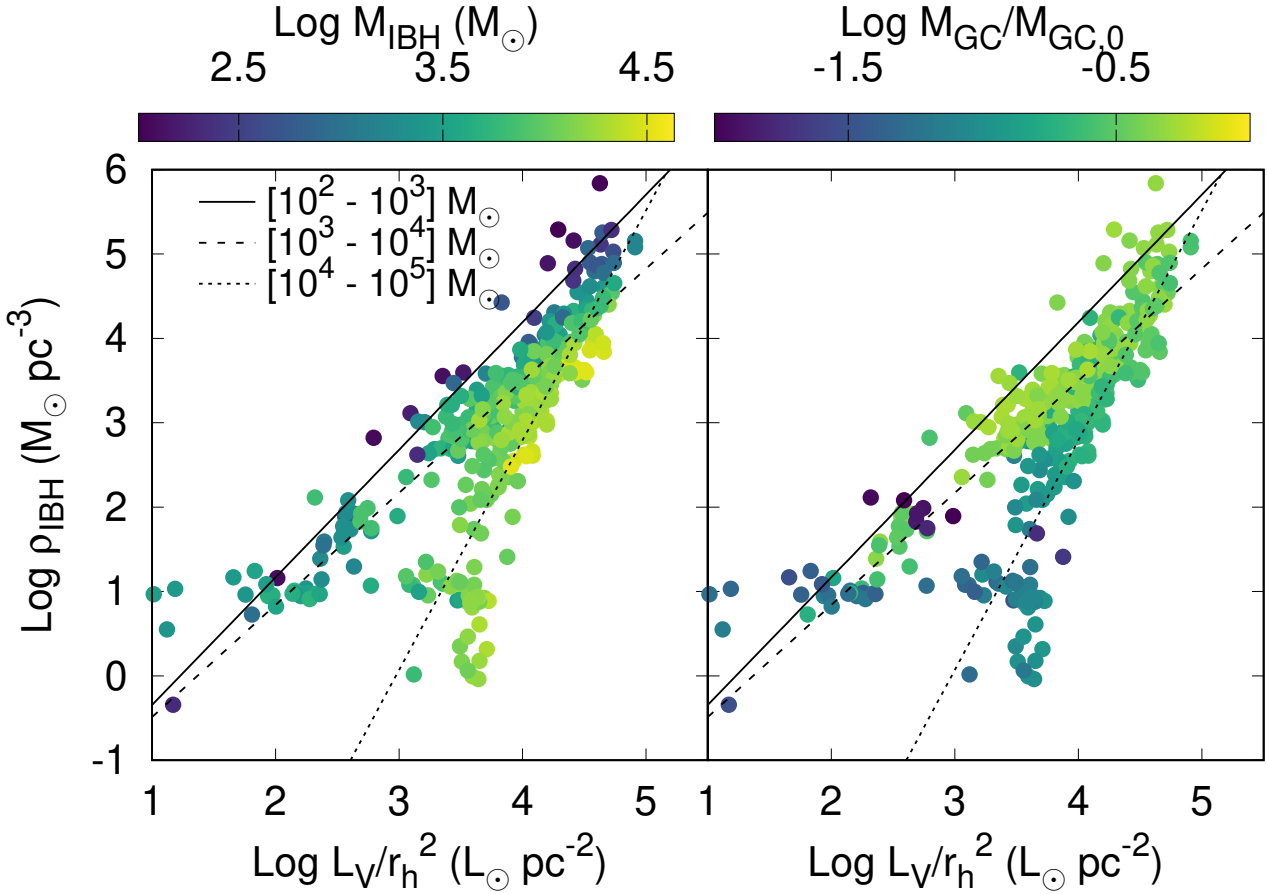


Figure 11. IMBHs fundamental plane: IMBH density as a function of the total visual luminosity divided by the square of the cluster observational half-mass radius. Different lines represent the best-fitting for models with IMBH masses in the range $10^2 < M_{\text{IMBH}}/M_{\odot} < 10^3$ (straight line), $10^3 < M_{\text{IMBH}}/M_{\odot} < 10^4$ (dashed line), and $10^4 < M_{\text{IMBH}}/M_{\odot} < 10^5$ (dotted line). Color-coding identifies the IMBH mass (left panel) or the ratio between final and initial values of the GC mass. Final quantities are taken at 12 Gyr.

allow to uniquely target potential IMBHs host candidates. Indeed as shown in our companion papers, GCs with similar properties might harbour an IMBH, a subsystem of stellar mass BHs, or be substantially *BH-free* (Arca Sedda et al. 2018; Askar et al. 2018).

One possibility is that GCs hosting different populations (an IMBH, a BH subsystem, or simply stars) arrange differently in the plane defined by different observables. Unfortunately, determining what observational parameters maximize the differences is not an easy task.

Figure 12 shows, for instance, how all MOCCA GCs distribute in the plane defined by half-mass radius and total visual luminosity, compared to actual Galactic GCs (as taken from Harris 2010, catalogue). Broadly speaking, our models gather in three distinct sectors of the plane, with IMBH-dominated GCs that occupy the region of large luminosities and moderate r_h values (1–5 pc). Models rich in stellar BHs occupy the same luminosity range, but are characterised by larger half-mass radius. Clusters that do not contain any appreciable BH population, instead, are characterised by a lower luminosity and a wide range of r_h values. Although the separation between these models is quite straightfor-

ward, it must be noted a considerable overlapping between all of them, especially in the region $L_V = 10^4 - 10^5 L_{\odot}$ and $r_h = 1 - 10$ pc. Unfortunately, this is the region where most of Galactic GCs lie. Another possible connection can be established between GCs luminosity and masses, as shown in Figure 13. The $M_{\text{GC}} - L_V$ plane is particularly interesting, as it shows a peculiar behaviour for GCs harbouring IMBHs surrounded by loose spheres of influence. MOCCA models having $\rho \gtrsim 3 \times 10^3$, as well as models containing a BH subsystem or stars-only, nicely distribute in the plane following a linear relation, as expected from simply converting the stellar mass in visual luminosity and vice-versa. Clusters with low-density spheres of influence, instead, significantly deviate from such relation, being characterized by a flatter distribution. Therefore, this kind of clusters appear less luminous than those with a similar mass and containing no-IMBH. Unfortunately, a direct comparison with observation is quite difficult owing to the intrinsically different methods used to calculate the luminosity from the mass (in theoretical models) and the mass from the luminosity (in observations).

Another possibility is to use only observed quantities,

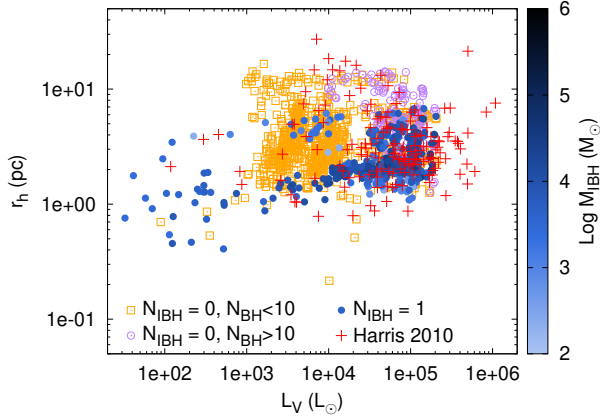


Figure 12. Observational half-mass radius as a function of the total visual luminosity for GCs in the [Harris \(2010\)](#) catalogue (red crosses) and for MOCCA models containing, at 12 Gyr, either no BHs (open green squares), at least 10 BHs with mass below 150 M_\odot (open purple points), or an IMBH (filled points). Colour-coding marks the IMBH mass, if present.

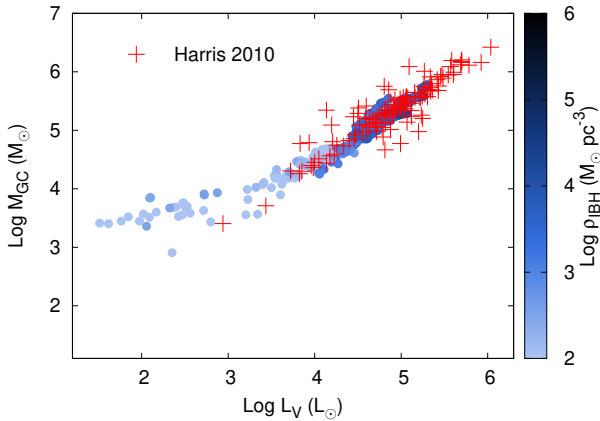


Figure 13. Present-day mass as a function of the total visual luminosity for Galactic GCs [Harris \(2010\)](#) (red crosses) and MOCCA models that contain an IMBH (coloured points). The color map identifies the influence sphere average density.

so to limit possible biases affecting their conversion into dynamical quantities. Figure 14 shows GCs central surface brightness Σ as a function of the average brightness used to define the fundamental plane, L_V/r_h^2 . We divided MOCCA models into those containing i) only a few BHs, ii) a BH subsystem, or iii) an IMBH, in order to better outline differences and similarities. The overlap between different models and Milky Way GCs is apparent, as well as the overlap between MOCCA models themselves. The inability to clearly distinguish between different models make hard to place constraints on possible IMBH-host candidates. However, as we will show in the next section, this can be done if a large set of observed quantities are taken into account simultaneously.

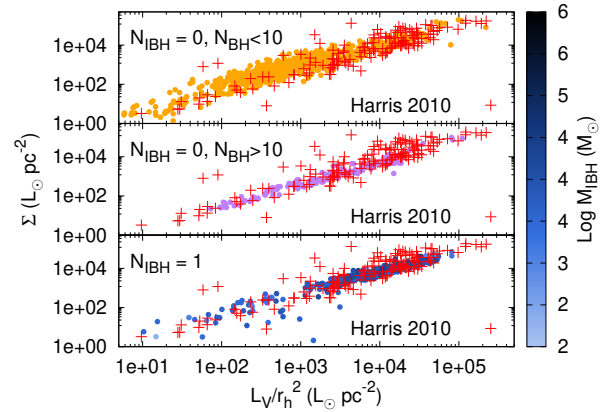


Figure 14. Central surface brightness as a function of the average surface brightness for Galactic GCs [Harris \(2010\)](#) (red crosses) and for MOCCA models. Top panel shows only MOCCA models that have less than 10 BHs and no IMBH at 12 Gyr. Central panel shows only models having at least 10 BHs. Bottom panel shows models harbouring an IMBH. Color coding identifies the IMBH mass, if present, or the mass of the heaviest BH.

5 A MULTI-DIMENSIONAL METHOD TO DISCERN GCS HOSTING IMBHS AND BHS

In order to identify what Galactic GCs are most likely hosting at present time a BHS or an IMBH, we use a technique that relies upon the minimization of the differences between observed and simulated quantities.

Indeed, MOCCA models aim at providing an overall representation of the Milky Way GC system, but they are not tailored to reproduce any of the observed Galactic GCs, thus a one-to-one correspondence between models and observations is unfeasible.

Therefore, to select MOCCA models that best reproduce a given GCs we calculate the norm

$$\|\mathcal{N}\| = \sqrt{(\Sigma_i (\Delta \mathcal{V}_i)^2)}, \quad (8)$$

being $\Delta \mathcal{V}_i$ the difference between the generic observable and the corresponding simulated quantity. For each Galactic GC, we identify the 10 nearest MOCCA models, i. e. with the smallest norm. We target GCs as BHS- or IMBH-host if at least 5 among the 10 closest MOCCA models harbour either more than 10 BHs (BHS-dominated) or a BH with mass $> 150 M_\odot$ (IMBH-dominated).

We calculate a 7-dimensional norm with components the GCs average surface brightness L_V/r_h^2 and central surface brightness Σ , the observational core radius, r_c ⁵, and half-light radius, r_h , the GCs Galactocentric distance, the

⁵ In order to calculate the observational core radius, we use the technique described in [Morscher et al. 2015](#) (see Appendix in [Morscher et al. 2015](#)) that fits the [King \(1962\)](#) model (see Equation 13 in [King \(1962\)](#) or equation A2 in [Morscher et al. \(2015\)](#)) to the cumulative luminosity of the cluster as a function of distance from the cluster centre. This binning-free technique obtains central surface brightness and core radius values that avoid random noise from bright stars that can be close to the IMBH and can drive up central surface brightness values.

visual L_V and bolometric luminosity L_B . All quantities are taken at 12 Gyr. Table A1 summarizes the results of the targeting procedure for all Galactic GCs⁶. For each GC, we use the scaling relations described here and in our companion paper (Arca Sedda et al. 2018) to infer either the number of BHs and the BHS or the IMBH mass.

In five cases, namely Whiting1, Pal1, Ko1, Ko2, and AM4, the GC luminosity has values below $\sim 3 \times 10^3 L_\odot$. In our MOCCA database, GCs containing an IMBH and having such low luminosities are characterized by influence radius almost constant $R_{\text{IBH}} \simeq 3.6 - 10$ pc. In this case, we used directly the $R_{\text{IBH}} - M_{\text{IBH}}$ relation, rather than using the density of the sphere of influence. Nonetheless, we note that the correlations predict very massive IMBHs compared to the GC observed mass and luminosity. Moreover, we show in previous sections that correlations tend to be much looser at GCs current masses below $\sim 1.5 \times 10^4 M_\odot$. Therefore, in the following we only consider GCs with a present day mass above $1.5 \times 10^4 M_\odot$ and visual luminosity $> 3 \times 10^3 L_\odot$.

Under this approximation and assuming the 7D norm, we find 35 GCs that might be harbouring an IMBH at present and 23 potentially containing a BHS. Models containing a BHS in this selection overlap pretty well with our previous paper (Askar et al. 2018), although the matching is not 100%. For 19 clusters we cannot say whether they host an IMBH or a BHS, while for the remaining 59 GCs our analysis do not suggest any significant central massive object. All these quantities are summarized in Table 2.

We show in Figure 15 the mass distribution of BHSs and IMBHs inferred for MW clusters. Despite the low number statistics, we find that the distribution of logarithmic IMBH mass can be described by a Gaussian

$$f(M_{\text{IBH}}) = \frac{a}{\sigma\sqrt{2\pi}} \exp\left[-\frac{(\text{Log}(M_{\text{IBH}}/M_\odot) - \mu)^2}{2\sigma^2}\right], \quad (9)$$

with $a = 0.14 \pm 0.3$, $\mu = 4.01 \pm 0.09$ and $\sigma = 0.4 \pm 0.1$. Most of IMBHs masses inferred with our approach exceed $10^3 M_\odot$.

Using MOCCA models, we find that the ratio $M_{\text{IBH}}/M_{\text{GC}}$ decreases at increasing the GC mass, as shown in Figure 16. Clearly, this relation affect the IMBH mass inferred for Galactic GCs. Indeed, out of the 35 shortlisted GCs, we find that 19 are characterized by $M_{\text{IBH}}/M_{\text{GC}} > 0.1$, 6 have $0.05 < M_{\text{IBH}}/M_{\text{GC}} < 0.1$, and the remaining 10 have $M_{\text{IBH}}/M_{\text{GC}} < 0.05$.

Possible GCs hosting an IMBH might be NGC1851 ($M_{\text{IBH}} \simeq 3.48 \times 10^3 M_\odot$), NGC6093 ($M_{\text{IBH}} \simeq 3.63 \times 10^3 M_\odot$), NGC6254 ($M_{\text{IBH}} \simeq 8.39 \times 10^3 M_\odot$). On the other hand GCs possibly harboring a noticeable number of BHs are NGC 3201 $N_{\text{BH}} \sim 113$ and NGC 6101 $N_{\text{BH}} \sim 147$, which are already known in literature as possible site with a large BH number.

The heaviest IMBH found through our analysis is hosted in NGC 6558, with an inferred mass of $M_{\text{IBH}} = 3.2 \times 10^4 M_\odot$, similar to the value inferred from microlensing measurements provided by Safonova & Shastri (2010), in NGC 6681 ($M_{\text{IBH}} \simeq 7.2 \times 10^3 M_\odot$), and NGC 6397

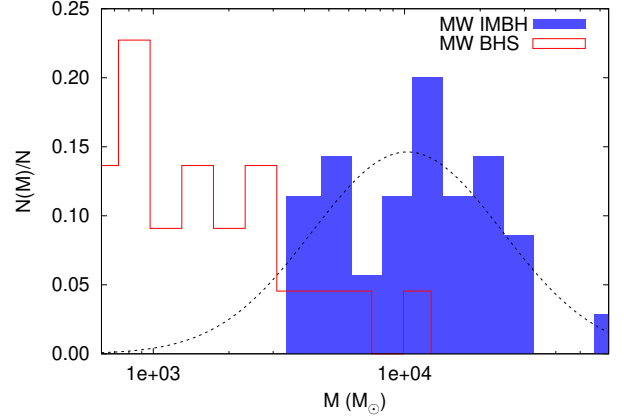


Figure 15. Mass distribution of central object for Galactic GCs containing an IMBH (blue filled steps), or a BHS (red open steps).

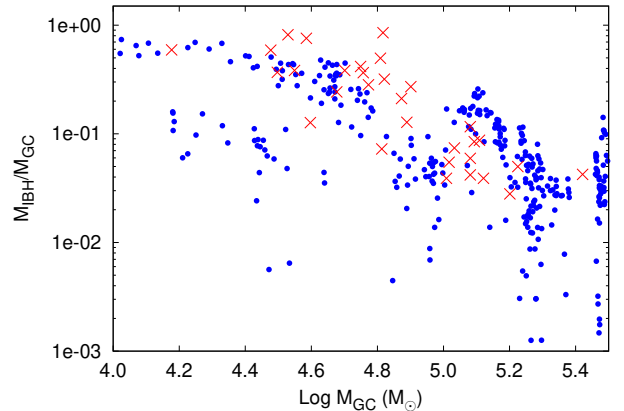


Figure 16. IMBH-to-GC mass ratio for MOCCA models (blue filled points) and for shortlisted Galactic GC (red crosses).

($M_{\text{IBH}} \simeq 9.9 \times 10^3 M_\odot$). Moreover, the procedure described here has the potential to be used for excluding the presence of an IMBH in GC. For instance, we found that cluster NGC 288 and NGC 5466 more likely host a BHS as massive as $2520 M_\odot$ and $4170 M_\odot$, rather than an IMBH, as suggested by earlier works (Lützgendorf et al. 2013b).

Our approach provides a rapid way to shortlist GCs which may be of potential interests for tailored numerical studies or further observational campaigns. However, we must note that the core radius might be ill-defined in presence of a central IMBH, while the typical luminosity and or central surface brightness can be dominated by the brightest stars in absence of a BHS, possibly causing misleading correspondence between models and observations. Therefore, we caution that a more careful analysis must be performed to assess whether a GC hosts an IMBH or a BHS.

⁶ Note that the total number in this table is smaller than the actual number of Milky Way GCs due to the constraints used in our selection procedure.

Table 2. Number of putative IMBH and BHS in Galactic GCs

N_{DIM}	parameters	N_{IBH}	N_{BHS}	N_{none}	N_{UNC}	N_{tot}
7D	$L_V/r_h^2, \Sigma, L_V, L_B, r_h, r_c, R_{GC}$	35	23	59	19	136

Col. 1: number of dimensions used to define the norm. Col. 2: quantities used to calculate the norm. Col. 3(4): Number of Galactic GCs containing an IMBH(BHS). Col. 5-6: Number of Galactic GCs that does not contain any central dark object, or for which a clear assesment cannot be made. Col 7: total number of GCs.

6 CONCLUSION

In this paper, we use the MOCCA SURVEY DATABASE I to dissect the interplay between IMBHs and their nursing GCs. Making use of over 2000 GC models, we show that it is possible to define a fundamental plane connecting the IMBH sphere of influence and the host GC luminosity and core radius. Our main results can be summarized as follows:

- we provide an extensive analysis of 407 MOCCA models containing an IMBH at 12 Gyr, characterizing each IMBH and its surrounding through the IMBH mass, influence radius, stellar density enclosed within the influence radius, and formation time.
- we show that IMBHs forming in MOCCA have typical masses $\sim 10^3 - 10^4 M_\odot$ characterized by an influence radii distribution peaking at ~ 3 pc, as shown in top and central panels of Figure 3;
- IMBHs formation time shows a clear bimodality that allows us to distinguish FAST (formation time smaller than 1 Gyr) and SLOW IMBHs. FAST IMBHs are, on average, heavier and surrounded by lower-mass stars compared to SLOW IMBHs (see bottom panel of Figure 3);
- we find that IMBH interactions with surrounding GC members drive the formation of a binary system in 32% of the cases, as shown in Figure 5, where the IMBH is bound to a MS star (13.7%), a WD (16.2%), a NS (0.2%), or a BH (2.7%). These systems are extremely important, as they can trigger tidal disruption events (in the case of MS), and the formation of intermediate mass ratio inspirals emitting GWs (for BHs) possibly in combination with explosive events and electromagnetic emission (for WDs and NSs). We list the main properties of GW sources candidates in Table 1;
- we find a striking correlation between IMBH mass and GC central density at 12 Gyr, provided that the GC mass at present time is above $5 \times 10^4 M_\odot$, as shown in Figure 6;
- we discover a population of *dark clusters*, i.e. clusters losing more than 90% of their mass, characterized by orbits within 3-5 kpc from the Galactic Centre. These class of clusters contain, on average, IMBHs with masses above $5 \times 10^3 M_\odot$, which constitutes more than 10% of the whole GC mass at 12 Gyr. Due to their low-orbits, these clusters can reach the Galactic Centre within a Hubble time, possibly dragging in there their IMBHs. These would nicely explain several recent observations of putative IMBHs orbiting the inner 10 pc of the Milky Way centre (see Figure 9);
- IMBHs forming via dynamical interactions in MOCCA can provide clues on the origin of SMBHs. We show that a fitting formula applied to MOCCA models and extended to the mass range of dwarf galaxies nicely overlap with a sample of observed low-mass AGN in dwarf galaxies (see Figure 10);

- we find a *fundamental plane* linking IMBH sphere of influence density and the host GC total luminosity and observational half-mass radius. We find two clear sequences in the fundamental plane. One sequence is defined by IMBHs with masses $< 10^4 M_\odot$ residing in GCs preserving more than 30% of their initial mass. The second sequence, instead, is dominated by heavier IMBHs, residing in clusters which underwent a severe mass loss, being $M_{GC}/M_{GC} < 0.3$. The fundamental plane is shown in Figure 11;

- we propose a simple tool to target Milky Way GCs possibly harbouring an IMBH at present. This concept relies upon the definition of a 7 dimensional space defined by GCs visual and bolometric total luminosity, half-mass and core radii, galactocentric distance, average and central surface luminosity. In this 7D space, for each Galactic GCs we find the 10 closest MOCCA models and calculate how many of them contain an IMBH, a BHS, or nothing. We shortlist 35(23) Galactic GCs possibly harbouring an IMBH(BHS) at present time, as summarized in Tables 2 and A1.

Our ranking procedure provides a simple and rapid tool to identify GCs hosting a central *dark* object (either an IMBH or a BH subsystem) and might be used to shortlist potential candidates to be observed with tailored observations.

In future works we will try to better constrain the discussed in the paper correlations using the new MOCCA models with updated physics and better determination of cluster parameters in the case of an IMBH presence.

7 ACKNOWLEDGMENTS

MAS also acknowledges financial support from the Alexander von Humboldt Foundation and the Federal Ministry for Education and Research in the framework of the research project “The evolution of black holes from stellar to galactic scales”, and the Sonderforschungsbereich SFB 881 “The Milky Way System” of the German Research Foundation (DFG). MAS acknowledges the Nicolaus Copernicus Astronomical Center in Warsaw for the hospitality given during the development of part of this research. MG was partially supported by the Polish National Science Center (NCN) through the grant UMO-2016/23/B/ST9/02732. AA is currently supported by the Carl Tryggers Foundation for Scientific Research through the grant CTS 17:113. This work benefited from support by the International Space Science Institute (ISSI), Bern, Switzerland, through its International Team programme ref. no. 393 The Evolution of Rich Stellar Populations & BH Binaries (2017-18).

REFERENCES

- Abbate F., Possenti A., Ridolfi A., Freire P. C. C., Camilo F., Manchester R. N., D’Amico N., 2018, *MNRAS*, **481**, 627
- Abbott B. P., et al., 2017, *Phys. Rev. D*, **96**, 022001
- Amaro-Seoane P., Gair J. R., Freitag M., Miller M. C., Mandel I., Cutler C. J., Babak S., 2007, *Classical and Quantum Gravity*, **24**, R113
- Anninos P., Fragile P. C., Olivier S. S., Hoffman R., Mishra B., Camarda K., 2018, *ApJ*, **865**, 3
- Antonini F., 2013, *ApJ*, **763**, 62
- Antonini F., Capuzzo-Dolcetta R., Mastrobuono-Battisti A., Merritt D., 2012, *ApJ*, **750**, 111
- Arca-Sedda M., 2016, *MNRAS*, **455**, 35
- Arca-Sedda M., Capuzzo-Dolcetta R., 2014a, *MNRAS*, **444**, 3738
- Arca-Sedda M., Capuzzo-Dolcetta R., 2014b, *ApJ*, **785**, 51
- Arca-Sedda M., Capuzzo-Dolcetta R., 2017, preprint, ([arXiv:1709.05567](https://arxiv.org/abs/1709.05567))
- Arca-Sedda M., Gualandris A., 2017, in prep.
- Arca-Sedda M., Capuzzo-Dolcetta R., Antonini F., Seth A., 2015, *ApJ*, **806**, 220
- Arca Sedda M., Askar A., Giersz M., 2018, *MNRAS*, **479**, 4652
- Askar A., Szkudlarek M., Gondek-Rosińska D., Giersz M., Bulik T., 2017a, *MNRAS*, **464**, L36
- Askar A., Bianchini P., de Vita R., Giersz M., Hypki A., Kamann S., 2017b, *MNRAS*, **464**, 3090
- Askar A., Arca Sedda M., Giersz M., 2018, *MNRAS*, **478**, 1844
- Askar A., Askar A., Pasquato M., Giersz M., 2019, *MNRAS*, **480**, 4684
- Ballone A., Mapelli M., Pasquato M., 2018, *MNRAS*, **480**, 4684
- Barack L., et al., 2018, arXiv e-prints,
- Bash F. N., Gebhardt K., Goss W. M., Vanden Bout P. A., 2008, *AJ*, **135**, 182
- Baumgardt H., Hut P., Makino J., McMillan S., Portegies Zwart S., 2003, *ApJ*, **582**, L21
- Baumgardt H., Gualandris A., Portegies Zwart S., 2006, *MNRAS*, **372**, 174
- Capuzzo-Dolcetta R., 1993, *ApJ*, **415**, 616
- Chen J.-H., Shen R.-F., 2018, *ApJ*, **867**, 20
- Chilingarian I. V., Katkov I. Y., Zolotukhin I. Y., Grishin K. A., Beletsky Y., Boutsia K., Osip D. J., 2018, *ApJ*, **863**, 1
- Colbert E. J. M., Ptak A. F., 2002, *ApJS*, **143**, 25
- Colpi M., Possenti A., Gualandris A., 2002, *ApJ*, **570**, L85
- Colpi M., Mapelli M., Possenti A., 2003, *ApJ*, **599**, 1260
- D’Amico N., Possenti A., Fici L., Manchester R. N., Lyne A. G., Camilo F., Sarkissian J., 2002, *ApJ*, **570**, L89
- Ebisuzaki T., et al., 2001, *ApJ*, **562**, L19
- Farrell S. A., et al., 2014, *MNRAS*, **437**, 1208
- Ferraro F. R., Possenti A., Sabbi E., Lagani P., Rood R. T., D’Amico N., Origlia L., 2003, *ApJ*, **595**, 179
- Fragione G., Ginsburg I., Kocsis B., 2017, preprint, ([arXiv:1711.00483](https://arxiv.org/abs/1711.00483))
- Fragione G., Leigh N. W. C., Ginsburg I., Kocsis B., 2018, *ApJ*, **867**, 119
- Fregeau J. M., Cheung P., Portegies Zwart S. F., Rasio F. A., 2004, *MNRAS*, **352**, 1
- Gaburov E., Gualandris A., Portegies Zwart S., 2008, *MNRAS*, **384**, 376
- Gebhardt K., Rich R. M., Ho L. C., 2005, *ApJ*, **634**, 1093
- Gieles M., Balbinot E., Yaaqib R. I. S. M., Hénault-Brunet V., Zocchi A., Peuten M., Jonker P. G., 2018, *MNRAS*, **473**, 4832
- Giersz M., Heggie D. C., Hurley J. R., 2008, *MNRAS*, **388**, 429
- Giersz M., Heggie D. C., Hurley J. R., Hypki A., 2013, *MNRAS*, **431**, 2184
- Giersz M., Leigh N., Hypki A., Lützgendorf N., Askar A., 2015, preprint, ([arXiv:1506.05234](https://arxiv.org/abs/1506.05234))
- Graham A. W., 2015, preprint, ([arXiv:1501.02937](https://arxiv.org/abs/1501.02937))
- Graham A. W., 2016, in Laurikainen E., Peletier R., Gadotti D., eds, *Astrophysics and Space Science Library* Vol. 418, Galactic Bulges. p. 263 ([arXiv:1501.02937](https://arxiv.org/abs/1501.02937)), doi:10.1007/978-3-319-19378-6_11
- Graham A. W., Spitler L. R., 2009, *MNRAS*, **397**, 2148
- Haas R., Shcherbakov R. V., Bode T., Laguna P., 2012, *ApJ*, **749**, 117
- Harris W. E., 2010, preprint, ([arXiv:1012.3224](https://arxiv.org/abs/1012.3224))
- Hopman C., Portegies Zwart S. F., Alexander T., 2004, *ApJ*, **604**, L101
- Hurley J. R., Tout C. A., Pols O. R., 2002, *MNRAS*, **329**, 897
- Hypki A., Giersz M., 2013, *MNRAS*, **429**, 1221
- Irwin J. A., et al., 2016, *Nature*, **538**, 356
- Kaaret P., Prestwich A. H., Zezas A., Murray S. S., Kim D.-W., Kilgard R. E., Schlegel E. M., Ward M. J., 2001, *MNRAS*, **321**, L29
- Kamann S., Wisotzki L., Roth M. M., Gerssen J., Husser T.-O., Sandin C., Weilbacher P., 2014, *A&A*, **566**, A58
- Kawana K., Tanikawa A., Yoshida N., 2018, *MNRAS*, **477**, 3449
- King I., 1962, *AJ*, **67**, 471
- Kızıltan B., Baumgardt H., Loeb A., 2017, *Nature*, **542**, 203
- Kormendy J., Ho L. C., 2013, *ARA&A*, **51**, 511
- Lanzoni B., et al., 2013, *ApJ*, **769**, 107
- Lin D., et al., 2018, *Nature Astronomy*, **2**, 656
- Lützgendorf N., et al., 2013a, *A&A*, **552**, A49
- Lützgendorf N., Baumgardt H., Kruijssen J. M. D., 2013b, *A&A*, **558**, A117
- MacLeod M., Goldstein J., Ramirez-Ruiz E., Guillochon J., Samsing J., 2014, *ApJ*, **794**, 9
- Maccarone T. J., Servillat M., 2008, *MNRAS*, **389**, 379
- Mandel I., Brown D. A., Gair J. R., Miller M. C., 2008, *ApJ*, **681**, 1431
- Mann C., et al., 2018, arXiv e-prints,
- Mapelli M., 2016, *MNRAS*, **459**, 3432
- Mastrobuono-Battisti A., Perets H. B., Loeb A., 2014, *ApJ*, **796**, 40
- Matsumoto H., Tsuru T. G., Koyama K., Awaki H., Canizares C. R., Kawai N., Matsushita S., Kawabe R., 2001, *ApJ*, **547**, L25
- Merritt D., 2013, Dynamics and Evolution of Galactic Nuclei
- Merritt D., Piatek S., Portegies Zwart S., Hemsendorf M., 2004, *ApJ*, **608**, L25
- Mezcua M., 2017, *International Journal of Modern Physics D*, **26**, 1730021
- Miller M. C., Colbert E. J. M., 2004, *International Journal of Modern Physics D*, **13**, 1
- Miller M. C., Hamilton D. P., 2002, *MNRAS*, **330**, 232
- Miller J. M., Fabian A. C., Miller M. C., 2004, *ApJ*, **614**, L117
- Morscher M., Pattabiraman B., Rodriguez C., Rasio F. A., Umbreit S., 2015, *ApJ*, **800**, 9
- Neumayer N., 2012, preprint, ([arXiv:1211.1795](https://arxiv.org/abs/1211.1795))
- Neumayer N., Walcher C. J., 2012, *Advances in Astronomy*, **2012**
- Noyola E., Gebhardt K., Kissler-Patig M., Lützgendorf N., Jalali B., de Zeeuw P. T., Baumgardt H., 2010, *ApJ*, **719**, L60
- Oka T., Tsujimoto S., Iwata Y., Nomura M., Takekawa S., 2017, *Nature Astronomy*, **1**, 709
- Peebles P. J. E., 1972, *ApJ*, **178**, 371
- Perera B. B. P., et al., 2017, *MNRAS*, **468**, 2114
- Perets H. B., Mastrobuono-Battisti A., 2014, *ApJ*, **784**, L44
- Peuten M., Zocchi A., Gieles M., Gualandris A., Hénault-Brunet V., 2016, *MNRAS*, **462**, 2333
- Portegies Zwart S. F., McMillan S. L. W., 2000, *ApJ*, **528**, L17
- Portegies Zwart S. F., McMillan S. L. W., 2007, in St.-Louis N., Moffat A. F. J., eds, *Astronomical Society of the Pacific Conference Series* Vol. 367, Massive Stars in Interactive Binaries. p. 597
- Portegies Zwart S. F., Baumgardt H., McMillan S. L. W., Makino J., Hut P., Ebisuzaki T., 2006, *ApJ*, **641**, 319
- Reines A. E., Comastri A., 2016, *Publ. Astron. Soc. Australia*, **33**, e054

- Rosswog S., Ramirez-Ruiz E., Hix W. R., Dan M., 2008, [Computer Physics Communications](#), **179**, 184
- Safonova M., Shastri P., 2010, [Ap&SS](#), **325**, 47
- Shen g.-F., 2019, [ApJ](#), **871**, L17
- Shen R.-F., Matzner C. D., 2014, [ApJ](#), **784**, 87
- Silk J., Arons J., 1975, [ApJ](#), **200**, L131
- Stodolkiewicz J. S., 1986, *Acta Astron.*, **36**, 19
- Strader J., Chomiuk L., Maccarone T. J., Miller-Jones J. C. A., Seth A. C., Heinke C. O., Sivakoff G. R., 2012, [ApJ](#), **750**, L27
- Takekawa S., Oka T., Iwata Y., Tokuyama S., Nomura M., 2017, [ApJ](#), **843**, L11
- Takekawa S., Oka T., Iwata Y., Tsujimoto S., Nomura M., 2019, [ApJ](#), **871**, L1
- Tremaine S. D., Ostriker J. P., Spitzer Jr. L., 1975, [ApJ](#), **196**, 407
- Tremou E., et al., 2018, [ApJ](#), **862**, 16
- Webb N., et al., 2012, [Science](#), **337**, 554
- Wiktorowicz G., Lasota J.-P., Middleton M., Belczynski K., 2018, arXiv e-prints,
- Wrobel J. M., Miller-Jones J. C. A., Nyland K. E., Maccarone T. J., 2018, in Kapinska A. D., ed., *The 34th Annual New Mexico Symposium*, held 9 November 2018 at the National Radio Astronomy Observatory. Edited by A.D. Kapinska. Online at http://www.aoc.nrao.edu/events/nmsymposium/2018/program.html, p.15. p. 15 ([arXiv:1806.06052](#))
- Zocchi A., Gieles M., Hénault-Brunet V., 2015, preprint, ([arXiv:1501.05262](#))
- Zocchi A., Gieles M., Hénault-Brunet V., 2017, [MNRAS](#), **468**, 4429
- Zocchi A., Gieles M., Hénault-Brunet V., 2019, [MNRAS](#), **482**, 4713
- van der Marel R. P., Anderson J., 2010, [ApJ](#), **710**, 1063

APPENDIX A: A

In Table A1 we show, for all the Galactic GCs, the probability to host an IMBH or a BHS assuming a 7D norm as explained in Section 5. Upon the definitions assumed here, we provide a label indicating whether the GC is likely to host an “IMBH”, a “BHS” or “NONE”, an estimate of BHs number (1 for IMBH), and the mass of the central dark object, either the IMBH or the BHS. For all target identified in [Askar et al. \(2018\)](#), for BHS, in the table we mark in red those that we find also with our new approach, in green those that gives an unclear results, in blue those that according to our approach should contain an IMBH, and in purple those that according to our approach should contain neither a BHS nor an IMBH.

Table A1: Galactic GCs probability to host an IMBH.

Red color marks GCs with BHS find also in [Askar et al. \(2018\)](#), green marks those giving unclear results, blue marks GCs in [Askar et al. \(2018\)](#) sample potentially harbouring an IMBH according to the new approach, purple marks those having no central dark object (IMBH or BHS).

ID	f_{none} %	f_{BHS} %	f_{IBH} %	central object	N_{BH}	M_{cen} $10^3 M_{\odot}$	M_{obs} $10^5 M_{\odot}$	$L_{\text{V,obs}}$ $10^5 L_{\odot}$
NGC104	80.0	0.0	20.0	NONE	-	-	10.02	5.01
NGC288	9.1	90.9	0.0	BHS	191 ± 41	2.52 ± 0.57	0.86	0.43
NGC362	58.2	0.0	41.8	NONE	-	-	4.03	2.01
Whiting1	0.0	0.0	100.0	IMBH	1	67.81 ± 19.02	0.02	0.01
NGC1261	1.8	52.7	45.5	BHS	74 ± 16	0.88 ± 0.20	2.25	1.13
Pal1	0.0	0.0	100.0	IMBH	1	38.36 ± 10.43	0.02	0.01
AM1	100.0	0.0	0.0	NONE	-	-	0.13	0.07
Eridanus	65.5	34.5	0.0	NONE	-	-	0.19	0.10
Pal2	0.0	43.6	56.4	IMBH	1	11.17 ± 2.64	2.64	1.32
NGC1851	20.0	16.4	63.6	IMBH	1	3.48 ± 0.91	3.67	1.84
NGC1904	94.5	5.5	0.0	NONE	-	-	2.38	1.19
NGC2298	40.0	0.0	60.0	IMBH	1	20.91 ± 4.80	0.57	0.29
NGC2419	0.0	100.0	0.0	BHS	205 ± 45	2.73 ± 0.62	10.02	5.01
Ko2	0.0	0.0	100.0	IMBH	1	63.04 ± 17.60	0.00	0.00
NGC2808	56.4	23.6	20.0	NONE	-	-	9.75	4.88
E3	0.0	0.0	100.0	IMBH	1	127.68 ± 30.78	0.08	0.04
Pal3	67.3	32.7	0.0	NONE	-	-	0.32	0.16
NGC3201	0.0	61.8	38.2	BHS	113 ± 24	1.41 ± 0.31	1.63	0.82
Pal4	49.1	50.9	0.0	BHS	645 ± 175	9.70 ± 2.77	0.43	0.22
Ko1	0.0	0.0	100.0	IMBH	1	64.29 ± 17.97	0.01	0.00
NGC4147	34.5	0.0	65.5	IMBH	1	19.23 ± 4.42	0.50	0.25
NGC4372	7.3	92.7	0.0	BHS	140 ± 29	1.79 ± 0.40	2.23	1.12
Rup106	74.5	16.4	9.1	NONE	-	-	0.59	0.30
NGC4590	20.0	38.2	41.8	UNCLEAR	-	-	1.52	0.76
NGC4833	9.1	5.5	85.5	IMBH	1	12.09 ± 2.84	3.17	1.58
NGC5024	49.1	21.8	29.1	UNCLEAR	-	-	5.21	2.61
NGC5053	30.9	69.1	0.0	BHS	397 ± 97	5.67 ± 1.44	0.87	0.43
NGC5139	7.3	65.5	27.3	BHS	57 ± 13	0.67 ± 0.16	0.00	10.86
NGC5272	32.7	16.4	50.9	IMBH	1	13.10 ± 3.07	6.10	3.05
NGC5286	92.7	0.0	7.3	NONE	-	-	5.36	2.68
AM4	20.0	0.0	80.0	IMBH	1	74.30 ± 20.96	0.01	0.00
NGC5466	27.3	72.7	0.0	BHS	301 ± 69	4.17 ± 1.00	1.06	0.53
NGC5634	80.0	9.1	10.9	NONE	-	-	2.04	1.02
NGC5694	61.8	0.0	38.2	NONE	-	-	2.32	1.16
IC4499	0.0	100.0	0.0	BHS	232 ± 51	3.13 ± 0.72	1.45	0.72
NGC5824	100.0	0.0	0.0	NONE	-	-	5.93	2.96
Pal5	100.0	0.0	0.0	NONE	-	-	0.20	0.10
NGC5897	0.0	100.0	0.0	BHS	197 ± 43	2.62 ± 0.59	1.33	0.67
NGC5904	32.7	21.8	45.5	UNCLEAR	-	-	5.72	2.86
NGC5927	100.0	0.0	0.0	NONE	-	-	2.28	1.14
NGC5946	96.4	0.0	3.6	NONE	-	-	1.27	0.64
BH176	32.7	0.0	67.3	IMBH	1	132.06 ± 31.92	0.07	0.04
NGC5986	9.1	85.5	5.5	BHS	52 ± 12	0.61 ± 0.15	4.06	2.03
Lynga7	21.8	0.0	78.2	IMBH	1	15.77 ± 3.66	0.75	0.37
Pal14	94.5	0.0	5.5	NONE	-	-	0.14	0.07
NGC6093	27.3	0.0	72.7	IMBH	1	3.63 ± 0.95	3.35	1.67
NGC6121	0.0	0.0	100.0	IMBH	1	11.21 ± 2.65	1.29	0.64
NGC6101	14.5	85.5	0.0	BHS	147 ± 31	1.89 ± 0.42	1.02	0.51
NGC6144	30.9	27.3	41.8	UNCLEAR	-	-	0.94	0.47
NGC6139	100.0	0.0	0.0	NONE	-	-	3.78	1.89
Terzan3	47.3	0.0	52.7	IMBH	1	46.44 ± 10.63	0.14	0.07
NGC6171	0.0	0.0	100.0	IMBH	1	14.01 ± 3.27	1.21	0.60
1636-283	1.8	0.0	98.2	IMBH	1	24.16 ± 5.52	0.07	0.03
NGC6205	9.1	54.5	36.4	BHS	58 ± 13	0.68 ± 0.16	4.50	2.25
NGC6229	14.5	72.7	12.7	BHS	65 ± 14	0.78 ± 0.18	2.86	1.43
NGC6218	18.2	61.8	20.0	BHS	71 ± 15	0.85 ± 0.20	1.44	0.72
FSR1735	30.9	0.0	69.1	IMBH	1	4.72 ± 1.20	0.65	0.33
NGC6235	43.6	0.0	56.4	IMBH	1	23.40 ± 5.35	0.56	0.28
NGC6254	0.0	30.9	69.1	IMBH	1	8.39 ± 2.02	1.68	0.84

Continued on next page

series Table A1 – continued from previous page

ID	7D norm			central object	N_{BH}	M_{cen} 10^3 M_{\odot}	M_{obs} 10^5 M_{\odot}	$L_{\text{V,obs}}$ 10^5 M_{\odot}
	f_{none} %	f_{BHS} %	f_{IBH} %					
NGC6256	16.4	0.0	83.6	IMBH	1	10.50 ± 2.49	1.24	0.62
Pal15	69.1	30.9	0.0	NONE	-	-	0.27	0.14
NGC6266	43.6	49.1	7.3	UNCLEAR	-	-	8.04	4.02
NGC6273	87.3	7.3	5.5	NONE	-	-	7.67	3.84
NGC6284	100.0	0.0	0.0	NONE	-	-	2.61	1.31
NGC6287	56.4	18.2	25.5	NONE	-	-	1.50	0.75
NGC6293	60.0	0.0	40.0	NONE	-	-	2.21	1.11
NGC6304	87.3	0.0	12.7	NONE	-	-	1.42	0.71
NGC6316	100.0	0.0	0.0	NONE	-	-	3.71	1.85
NGC6341	100.0	0.0	0.0	NONE	-	-	3.29	1.64
NGC6325	14.5	0.0	85.5	IMBH	1	5.69 ± 1.42	1.04	0.52
NGC6333	40.0	21.8	38.2	UNCLEAR	-	-	2.59	1.29
NGC6342	65.5	0.0	34.5	NONE	-	-	0.63	0.32
NGC6356	34.5	29.1	36.4	UNCLEAR	-	-	4.34	2.17
NGC6355	54.5	0.0	45.5	NONE	-	-	2.89	1.45
NGC6352	38.2	0.0	61.8	IMBH	1	21.10 ± 4.84	0.66	0.33
IC1257	83.6	0.0	16.4	NONE	-	-	0.49	0.25
Terzan2	21.8	0.0	78.2	IMBH	1	29.15 ± 6.65	0.38	0.19
NGC6366	18.2	0.0	81.8	IMBH	1	27.60 ± 6.30	0.34	0.17
Terzan4	12.7	0.0	87.3	IMBH	1	77.39 ± 18.05	0.11	0.05
HP1	10.9	0.0	89.1	IMBH	1	55.98 ± 12.87	0.66	0.33
NGC6362	32.7	40.0	27.3	UNCLEAR	-	-	1.03	0.52
NGC6380	85.5	14.5	0.0	NONE	-	-	1.71	0.86
Terzan1	0.0	0.0	100.0	IMBH	1	178.58 ± 44.30	0.10	0.05
Ton2	52.7	0.0	47.3	NONE	-	-	0.50	0.25
NGC6388	45.5	49.1	5.5	UNCLEAR	-	-	9.93	4.97
NGC6402	20.0	50.9	29.1	BHS	46 ± 10	0.53 ± 0.13	7.47	3.73
NGC6401	63.6	10.9	25.5	NONE	-	-	2.47	1.24
NGC6397	12.7	0.0	87.3	IMBH	1	9.89 ± 2.36	0.77	0.39
Pal6	52.7	0.0	47.3	NONE	-	-	0.89	0.44
NGC6426	69.1	5.5	25.5	NONE	-	-	0.80	0.40
Djorg1	78.2	1.8	20.0	NONE	-	-	1.06	0.53
Terzan5	1.8	0.0	98.2	IMBH	1	4.45 ± 1.14	1.59	0.79
NGC6440	45.5	49.1	5.5	UNCLEAR	-	-	5.41	2.70
NGC6441	49.1	49.1	1.8	UNCLEAR	-	-	12.16	6.08
Terzan6	50.9	0.0	49.1	NONE	-	-	1.86	0.93
NGC6453	45.5	0.0	54.5	IMBH	1	5.15 ± 1.30	1.32	0.66
NGC6496	32.7	67.3	0.0	BHS	98 ± 20	1.20 ± 0.27	1.30	0.65
Terzan9	0.0	0.0	100.0	IMBH	1	40.88 ± 9.33	0.05	0.03
Djorg2	34.5	0.0	65.5	IMBH	1	8.00 ± 1.94	1.08	0.54
NGC6517	61.8	10.9	27.3	NONE	-	-	3.41	1.71
Terzan10	49.1	0.0	50.9	IMBH	1	16.75 ± 3.87	0.59	0.30
NGC6522	54.5	0.0	45.5	NONE	-	-	1.96	0.98
NGC6535	50.9	0.0	49.1	NONE	-	-	0.14	0.07
NGC6528	72.7	0.0	27.3	NONE	-	-	0.73	0.36
NGC6539	32.7	29.1	38.2	UNCLEAR	-	-	3.54	1.77
NGC6544	21.8	0.0	78.2	IMBH	1	3.98 ± 1.03	1.02	0.51
NGC6541	83.6	0.0	16.4	NONE	-	-	4.38	2.19
2MS-GC01	0.0	0.0	100.0	IMBH	1	11.56 ± 2.73	0.48	0.24
ESO-SC06	98.2	0.0	1.8	NONE	-	-	0.15	0.08
NGC6553	40.0	12.7	47.3	UNCLEAR	-	-	2.19	1.10
2MS-GC02	0.0	0.0	100.0	IMBH	1	8.90 ± 2.14	0.15	0.08
NGC6558	16.4	0.0	83.6	IMBH	1	31.96 ± 7.28	0.64	0.32
IC1276	21.8	0.0	78.2	IMBH	1	21.64 ± 4.96	0.80	0.40
Terzan12	0.0	0.0	100.0	IMBH	1	18.99 ± 4.37	0.08	0.04
NGC6569	50.9	40.0	9.1	NONE	-	-	3.51	1.75
BH261	0.0	0.0	100.0	IMBH	1	18.30 ± 4.22	0.08	0.04
NGC6584	30.9	69.1	0.0	BHS	69 ± 15	0.83 ± 0.19	2.04	1.02
NGC6624	52.7	0.0	47.3	NONE	-	-	1.69	0.85
NGC6626	74.5	0.0	25.5	NONE	-	-	3.14	1.57
NGC6638	23.6	0.0	76.4	IMBH	1	5.05 ± 1.27	1.21	0.60
NGC6637	56.4	38.2	5.5	NONE	-	-	1.95	0.97
NGC6642	87.3	0.0	12.7	NONE	-	-	0.79	0.39

Continued on next page

series Table A1 – continued from previous page

ID	7D norm			central object	N_{BH}	M_{cen} 10^3 M_{\odot}	M_{obs} 10^5 M_{\odot}	$L_{\text{V,obs}}$ 10^5 M_{\odot}
	f_{none} %	f_{BHS} %	f_{IBH} %					
NGC6652	85.5	0.0	14.5	NONE	-	-	0.79	0.39
NGC6656	25.5	40.0	34.5	UNCLEAR	-	-	4.30	2.15
Pal8	61.8	0.0	38.2	NONE	-	-	0.27	0.14
NGC6681	20.0	0.0	80.0	IMBH	1	7.17 ± 1.75	1.21	0.60
GLIMPSE01	34.5	0.0	65.5	IMBH	1	5.01 ± 1.27	0.40	0.20
NGC6712	14.5	58.2	27.3	BHS	70 ± 15	0.84 ± 0.19	1.71	0.86
NGC6715	98.2	1.8	0.0	NONE	-	-	16.79	8.39
NGC6717	45.5	0.0	54.5	IMBH	1	11.56 ± 2.73	0.31	0.16
NGC6723	45.5	21.8	32.7	UNCLEAR	-	-	2.32	1.16
NGC6749	52.7	0.0	47.3	NONE	-	-	0.82	0.41
NGC6752	61.8	0.0	38.2	NONE	-	-	2.11	1.06
NGC6760	41.8	45.5	12.7	UNCLEAR	-	-	2.34	1.17
NGC6779	30.9	65.5	3.6	BHS	81 ± 17	0.98 ± 0.22	1.57	0.79
Terzan7	60.0	0.0	40.0	NONE	-	-	0.17	0.09
Pal10	0.0	0.0	100.0	IMBH	1	13.56 ± 3.17	0.35	0.18
Arp2	92.7	7.3	0.0	NONE	-	-	0.22	0.11
NGC6809	5.5	94.5	0.0	BHS	108 ± 23	1.34 ± 0.30	1.82	0.91
Terzan8	69.1	21.8	9.1	NONE	-	-	0.18	0.09
Pal11	47.3	49.1	3.6	UNCLEAR	-	-	1.00	0.50
NGC6838	0.0	0.0	100.0	IMBH	1	17.67 ± 4.08	0.30	0.15
NGC6864	100.0	0.0	0.0	NONE	-	-	4.58	2.29
NGC6934	41.8	47.3	10.9	UNCLEAR	-	-	1.63	0.82
NGC6981	36.4	29.1	34.5	UNCLEAR	-	-	1.12	0.56
NGC7006	21.8	60.0	18.2	BHS	120 ± 25	1.52 ± 0.34	2.00	1.00
NGC7078	89.1	0.0	10.9	NONE	-	-	8.11	4.06
NGC7089	76.4	9.1	14.5	NONE	-	-	7.00	3.50
NGC7099	72.7	0.0	27.3	NONE	-	-	1.63	0.82
Pal12	0.0	0.0	100.0	IMBH	1	232.65 ± 59.21	0.10	0.05
Pal13	16.4	0.0	83.6	IMBH	1	75.41 ± 17.57	0.05	0.03
NGC7492	70.9	16.4	12.7	NONE	-	-	0.36	0.18

This paper has been typeset from a \LaTeX file prepared by the author.